https://doi.org/10.5194/egusphere-2026-3797
Preprint. Discussion started: 31 August 2026

Understanding the sources and variability of methane emissions in Madrid with Sentinel-5P TROPOMI, GHGSat, and aircraft observations

Daniel A. Potts[1*], Harjinder Sembhi[1], Matthieu Dogniaux[2], Joannes D. Maasakkers[2], Berend J. Schuit[2] Dirk Schuettemeyer[3], Timon Hummel[3], Rocio Barrio Guillo[1], Oliver Schneising[4], Luis Guanter[5], Ilse Aben[2]

1 University of Leicester, UK
2 SRON Space Research Organisation Netherlands, Leiden, the Netherlands
3 European Space Agency
4 Institute of Environmental Physics, University of Bremen, Bremen, Germany
5 Universitat Politècnica de València (UPV), Spain
[*] *dap33@leicester.ac.uk*

1 Abstract

Routine, passive monitoring using satellite sensors offers an effective means of understanding the location, frequency and intensity of industrial methane emissions. Satellites have been used largely to identify fugitive point source emissions in sectors such as oil and gas, but their efficacy for more diffuse sources such as landfills is less established, and formal integration into official reporting and compliance frameworks has yet to be achieved. A persistent methane hotspot originating from Madrid was identified using TROPOMI, where it remains one of the largest signals in Europe. Two landfills, Las Dehesas and Pinto, were identified as significant contributors based on GHGSat observations.

This study presents a comprehensive analysis of the TROPOMI and GHGSat observational record up to 2024 for Madrid, alongside aircraft observations, all contextualised against previous short-term studies, facility-scale reporting, and gridded inventories. Plume-based city-scale emissions averaged 13 ± 9 t/hr from TROPOMI compared to ~8 t/hr from the gridded inventories. Facility-scale emissions ranged from 2.5 ± 1.3 t/hr (Las Dehesas) and 3.8 ± 2.0 t/hr (Pinto) from GHGSat, and 3.0 ± 1.8 to 4.6 ± 2.7 t/hr respectively from aircraft, compared to reported averages of 0.4 and 1.0 t/hr between 2018–2024. Measurement-derived rates exceeded reported estimates by a factor of 0.5–6, highlighting a severe gap between bottom-up inventory and top-down observational approaches. We discuss challenges associated with satellite interpretation and meteorology, connect emissions to on-site management practices, and make recommendations towards operational use of these datasets.

https://doi.org/10.5194/egusphere-2026-3797
Preprint. Discussion started: 31 August 2026

30 **Graphical Abstract**

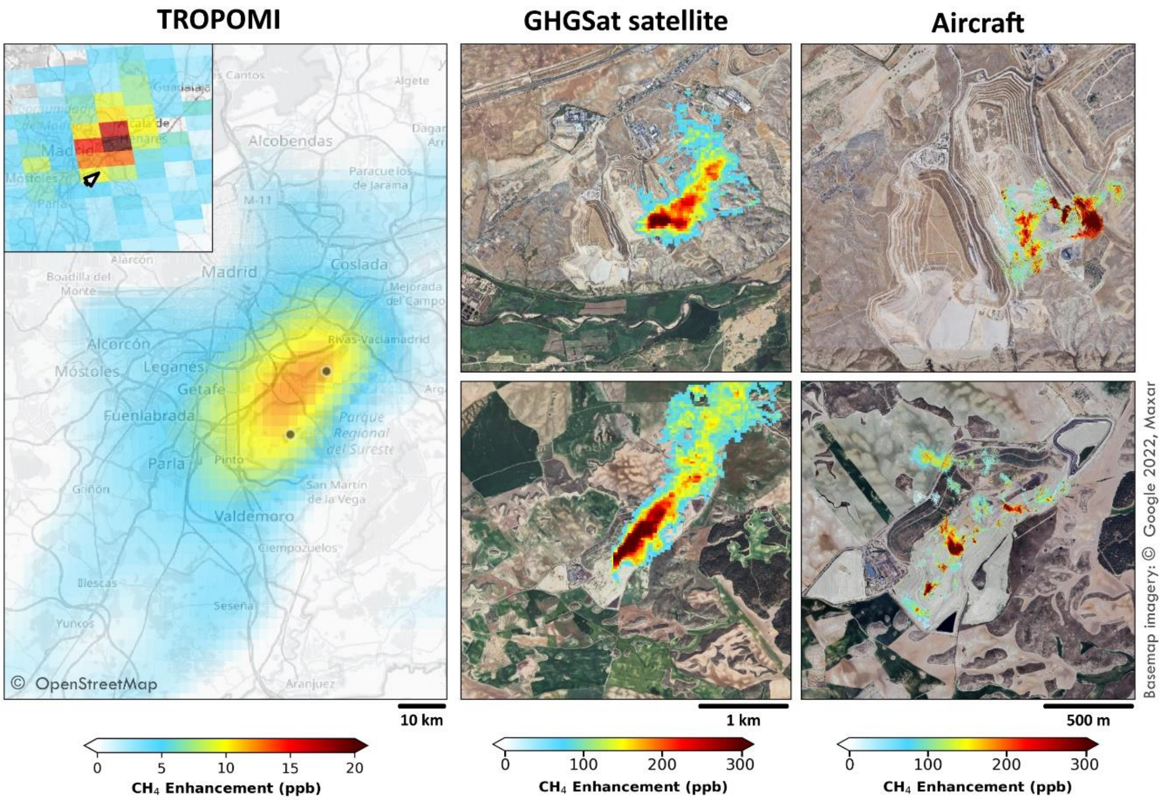

https://doi.org/10.5194/egusphere-2026-3797
Preprint. Discussion started: 31 August 2026

2 Introduction

Methane (CH_4) is a potent greenhouse gas with a global warming potential more than 80 times higher than carbon dioxide (CO_2) over 20 years and has contributed ~30% to global temperature rise since the 1800's (Nisbet-Jones et al., 2022). There has been an overall upward trend of atmospheric methane since industrial times, largely driven by increased anthropogenic emissions (Skeie et al., 2023). Anthropogenic sources of methane are estimated to contribute approximately 60% (equivalent to 359 Tg CH_4 yr−1) to the total global methane budget, including sources such as agriculture (enteric fermentation and manure, rice cultivation), fossil fuels (coal mining, oil, gas and industry), and waste (landfills and wastewater treatment) (Saunois et al., 2025). The recent Global Methane Budget 2000 –2020 estimates that the landfill and waste sector contributes approximately 19% to the global anthropogenic budget (Saunois et al., 2025).

Satellites have been shown to reliably detect CH_4 emissions from national and regional scales down to individual industrial facilities, and can provide valuable insight into the location and intensity of anthropogenic CH_4 emissions. The European Space Agency's Sentinel-5P TROPOspheric Monitoring Instrument (TROPOMI), launched in 2017, provides daily, near global coverage with a swath width of 2600 km and spatial pixel footprint of 7 x 7 km at nadir (improved to 5.5 x 7 km as of August 2019). Regional and large-source methane emission fluxes have been quantified with TROPOMI for a range of sectors including coal mines (Sadavarte et al., 2021; Tu et al., 2022b; Yang et al., 2026), oil and gas facilities (Gao et al., 2023; Schneising et al., 2020; Schuit et al., 2023; Shen et al., 2023; Veefkind et al., 2023), and more recently from urban areas with landfill sites (Dogniaux et al., 2025; Maasakkers et al., 2022; Nesser et al., 2024; Tu et al., 2022a, Zhang et al., 2025). Complementarily, compact, targeted satellites, such as the GHGSat constellation, can identify CH_4 plumes at high resolution (~ 25 m), and are capable of attributing CH_4 plumes directly to facility, and often sub-facility, assets, albeit at the compromise of daily global coverage (Jervis et al., 2021; Varon et al., 2019). In addition, there are an increasing number of airborne sensors capable of 1 - 5 m resolution observations, allowing individual sub-facility leaks to be identified during dedicated aircraft campaigns (El Abbadi et al., 2024; Cusworth et al., 2024; Krautwurst et al., 2025).

Urban CH_4 emission plumes are primarily a combination of waste management (waste water, landfills), gas management (natural gas, domestic heating etc.), and road transport emissions (Defratyka et al., 2021; Townsend-Small et al., 2012), with landfills typically being the majority contributor when present. Madrid presents as one of the strongest urban methane enhancements in Europe, with methane plumes frequently observed by TROPOMI (Schuit et al., 2023). Targeted observations by GHGSat attributed a large portion of this urban emission plume to two municipal waste landfills located ~12 km south-east from Madrid city centre, known as Las Dehesas landfill and Pinto landfill.

Organic waste in landfills decomposes slowly over many years, where it produces varying levels of decomposition landfill gas (LFG) and contaminated wastewater known as leachate. LFG consists mostly of methane (~55%) and carbon dioxide (40%) for a mature landfill, both of which are important greenhouse gases (GHGs) (Kashyap et al., 2016). Methane emissions from landfills are biogenic, driven by microbial anaerobic decomposition of waste. Waste within landfills generally reach a state of high, consistent methane production within 300 days, when the environment is sufficiently anaerobic, and will

https://doi.org/10.5194/egusphere-2026-3797
Preprint. Discussion started: 31 August 2026

continue to produce methane for decades under controlled conditions until the waste is bio-stable (Kurniawan et al., 2022; Meyer-Dombard et al., 2020). LFG production is dependent on (i) physical characteristics such as cell size, layer depth, membrane material, barrier condition and presence of onsite gas capture systems etc.), (ii) conditions favourable to microbial activity, namely; waste composition, anaerobic state, temperature, moisture content and (iii) local meteorological conditions, particularly surface/atmospheric pressure, as well as air temperature, humidity and wind (Aghdam et al., 2019; Czepiel et al., 2003; Duan et al., 2022; Kissas et al., 2022; Kurniawan et al., 2022; Poulsen Tjalfe G. et al., 2003).

Landfills are constructed incrementally as a series of connected but discrete cells, which allows completed cells to be capped and for gas to be extracted whilst the next cell is constructed. Operational landfills therefore typically have a combination of complete and capped cells, recently completed cells undergoing capping, and an active/working cell. Fugitive emissions (those that are not captured) originate from completed/capped landfill cells through diffuse emission through the cover (Bogner et al., 2011; Sirimangkhala et al., 2018; Zhang et al., 2012), slope leakage when there is insufficient cover (porosity, permeability, diffusivity), breakage of cover (fissures, cracks), or through infrastructure (well maintenance issues, degradation of gas collection infrastructure) (Allen et al., 2019; Emran et al., 2017; Scheutz et al., 2011). For active cells, fugitive emissions originate from diffuse transport between the waste and the cover material, and typically through the current working face. Active cells cannot be constantly sealed during construction, as waste is added daily, and therefore can act as diffuse heterogeneous sources of methane. The active cell typically accounts for a significant portion of the total emission, with estimates ranging from 76% of total emissions for facilities with gas capture to 38% for facilities without (Omidi et al., 2025; Scarpelli et al., 2024).

Measurement of landfill CH_4 emissions can be challenging, as landfills act as a heterogenous and variable mix of point and area sources (Maasakkers et al., 2022). There can be large spatial and temporal variations in the measured emission rate driven by changes in environmental conditions, operational practices, landfill status, and observational sensitivities (Agency, 2024; Rachor et al., 2013; Srikanth et al., 2025.). Deriving whole site emissions for landfills using bottom-up modelling approaches can be challenging and uncertain due to assumptions made in the bio-availability of the waste deposited, the rate of gas production, and the efficiency of gas capture (Ganesan et al., 2019). In-situ, aircraft and satellite measurements have repeatedly shown emissions for individual landfills can be larger than estimated emissions from regulatory-grade bottom-up methods by a factor of 2-3 (Dogniaux et al., 2025; Giordano et al., 2024; Nesser et al., 2024; Wang et al., 2024), highlighting the need for frequent and reliable measurement-based evidence to evaluate and complement traditional approaches.

Satellites are well positioned to fill a vital gap in emission monitoring by providing global, repeated, and independent evaluations of emissions from regulated facilities. Whilst satellites have been validated for point sources via numerous controlled release experiments (Sherwin et al., 2023, 2024), experimental design for controlled releases for diffuse area sources is much more complex, with the first landfill-type diffuse controlled release facility only coming online in recent years (FluxLab, 2026; Iftakhar Hossain et al., 2025). In addition, understanding the sources of variability in emissions derived from different satellites and data providers can be improved through intercomparisons (Eldering, 2026; Sherwin et al., 2023; Zhang et al., 2025). For example, to evaluate whether part of the variability is synthetic (e.g. related to decisions in wind

https://doi.org/10.5194/egusphere-2026-3797
Preprint. Discussion started: 31 August 2026

interpretation/calibration, retrieval, plume delineation, observation frequency) or sensitivity-related (e.g. detection limit, spatial scales, fractional sensitivity to total emission, influence of fine-scale turbulence).

This study presents a comprehensive multi-year multi-instrument analysis of methane emissions over Madrid using satellite and aircraft observations. We explore the dominant contributing sources to this enhanced urban signal, examine the influence of meteorology on satellite-derived emission estimates, and investigate the relationship between landfill operational activity and emission origin, providing measurement-based constraints on Madrid's methane budget which are necessary to evaluate and improve upon traditional inventory approaches.

3 Materials and Methods

3.1 Study area

Madrid is located at the centre of the Iberian Peninsula on the expansive Meseta Central plateau (645 m above sea level), with a metropolitan population of approximately 7 million people, making the Spanish capital one of the highest and most populous cities in Europe. The city sits at the north-eastern end of the Tagus River basin, flanked to the north, east, and west by mountain ranges. Madrid contains a combination of active and closed Municipal Solid Waste (MSW) landfills and a number of Waste Water Treatment Plants (WWTP), not uncommon for a city of this size. A significant fraction of the regions municipal waste will arrive at one of Madrid's two largest active landfills; Las Dehesas (40.324° N, 3.590° W) or Pinto (40.264° N, 3.631° W), shown in Figure 1. They are both located south-east from Madrid city centre, 6 km apart from each other. Las Dehesas landfill is owned by the Madrid City Council and serves the city of Madrid (approx. 3.5 million people) The Las Dehesas landfill is part of the broader Valdemingomez Technology Park (VTP), a collection of waste management facilities including active and completed landfill sites, waste sorting/recycling facilities, anaerobic digestion plants and a biogas upgrading plant (PTB). Pinto is owned by Mancomunidad del Sur and serves 66 municipalities to the South of Madrid city (approx. 2 million people). The majority of the landfills in the VTP, section LD-1 of Las Dehesas and section P-1 of Pinto have been completed for 5+ years (Figure 1). LD-2/3 of Las Dehesas and the P-2/4 Pinto were under active construction at some stage between 2021 - 2024. West of Las Dehesas is La Salmedina, a construction and demolition waste landfill separate to the VTP not expected to generate methane.

Waste handled before arrival or at these landfills undergo some degree of Mechanical and Biological Treatment (MBT). Mechanical treatments can include sorting, separation, recycling, and recovery stages, to limit the volume of waste sent to landfill. Biological treatments include aerobically-accelerated composting for low quality organics and anaerobic digestion for high quality organics, where waste is broken down in an enclosed controlled system to extract high quality methane directly and to biostablise the waste before landfill. MBT is designed to increase recycling and reclamation, reduce emissions, and to generate revenue from recovered recyclable materials and energy. Both sites have LFG extraction systems and generate electricity via on-site biogas-fired engines. The VTP also upgrades biogas produced in anaerobic digesters into biomethane via the PTB, which is then fed into the gas transport grid. Between these landfills are two WWTP (40.312° N, -

https://doi.org/10.5194/egusphere-2026-3797
Preprint. Discussion started: 31 August 2026

3.615° W and 40.300° N, -3.602° W), owned by Canal de Isabel II, which may also contribute to locally elevated methane concentrations.

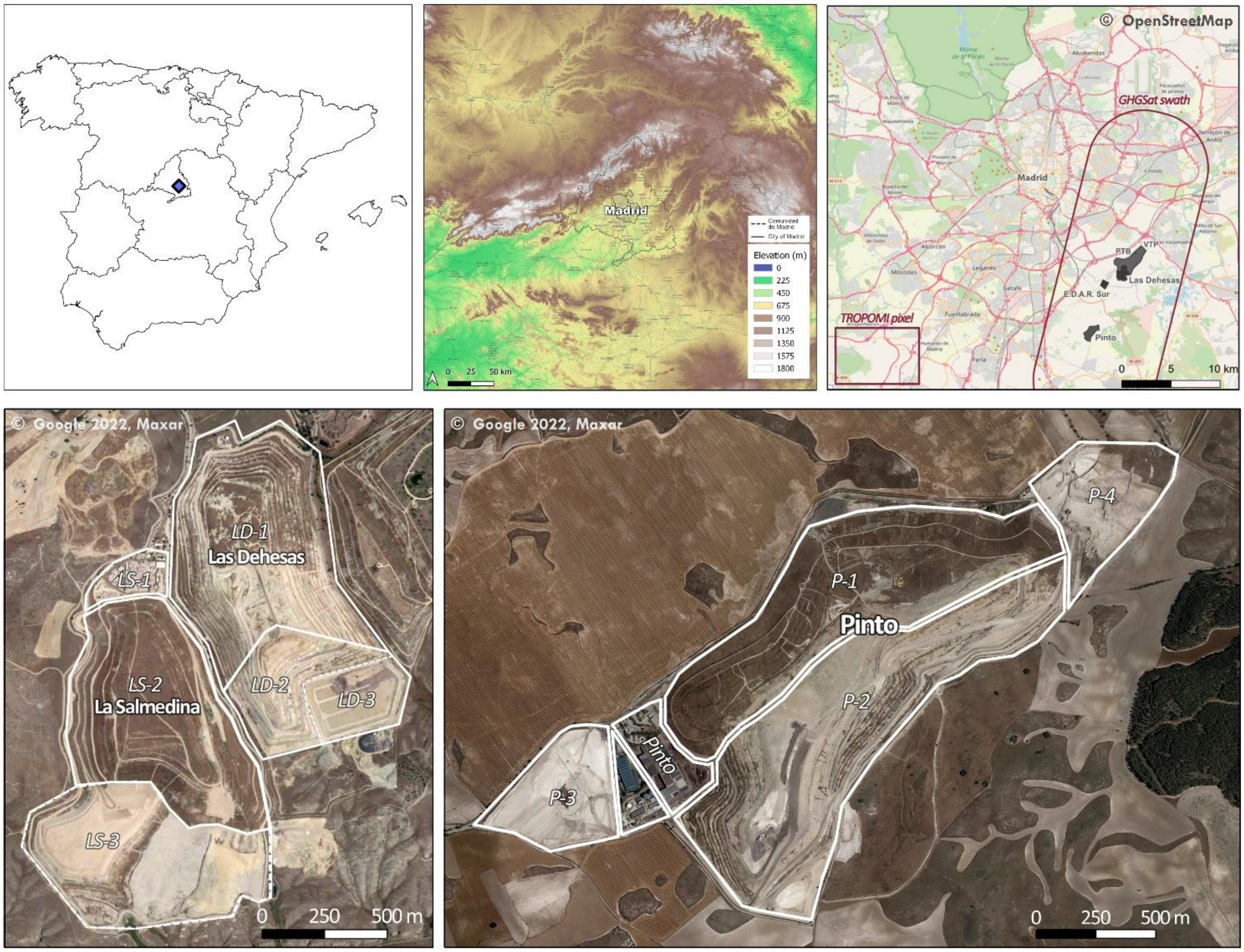

Figure 1: Contextual overview of the study region, from national (top left), to regional (top centre – Madrid with topography from Copernicus GLO-90), to city (top right – Metropolitan area of Madrid with facilities and satellite swaths marked). Lower panels show Las Dehesas (bottom left) and Pinto (bottom right), with subregions drawn based on observed activity and have been defined for this study. These cells are not the naming convention used by the facility.

https://doi.org/10.5194/egusphere-2026-3797
Preprint. Discussion started: 31 August 2026

3.2 Datasets and Methods

3.2.1 TROPOMI

This study uses data from the TROPOspheric Monitoring Instrument (TROPOMI) on-board Sentinel-5P, a push-broom imagining spectrometer with a resolution of 5.5 x 7 km at nadir for SWIR wavelengths. There are two Level-2 TROPOMI data products available: the ESA operational product (using the SRON operational retrieval code, Lorente et al., 2021, 2023) and the Bremen IUP scientific product (Schneising et al., 2026). These algorithms employ different radiative transfer models, spectroscopy, quality filters, retrieved parameters and post-processing correction of albedo bias, and therefore offer slightly different interpretations of the methane total column (noted XCH4). For this study, the ESA v2.4.0 – v2.8.0 and Bremen IUP-UB TROPOMI/WFMD v2.0 products were used in parallel. The ESA operational product was analysed using a machine learning approach (ESA_{ML}, Schuit et al., 2023), and through a statistics-based masking approach (ESA_{SB}). The IUP-UB WFMD product was analysed by the statistics-based approach only ($IUP\text{-}UB_{SB}$). Both methods are detailed in the supplement (section A.1). Source rates were quantified using the Integrated Mass Enhancement (IME) method used extensively for satellite CH_4 emission quantification (Varon et al., 2018). Emissions were calculated using wind information from GEOS-FP 10m (Molod et al., 2012), ERA5 10m, and ERA5 PBL (Hersbach et al., 2020), using effective wind calibrations from (Schuit et al., 2023). An ensemble mean of these per-wind quantifications was used as the final emission rate for each approach. Plumes consisting of less than 3 pixels were discarded. Figure 2 demonstrates a typical TROPOMI observation including supplemental information such as elevation, albedo, wind history and the vertical wind profile to aid in the interpretation of each plume. Two data products, two distinct methods, and three wind sources were used to show the impact of these choices on derived emissions.

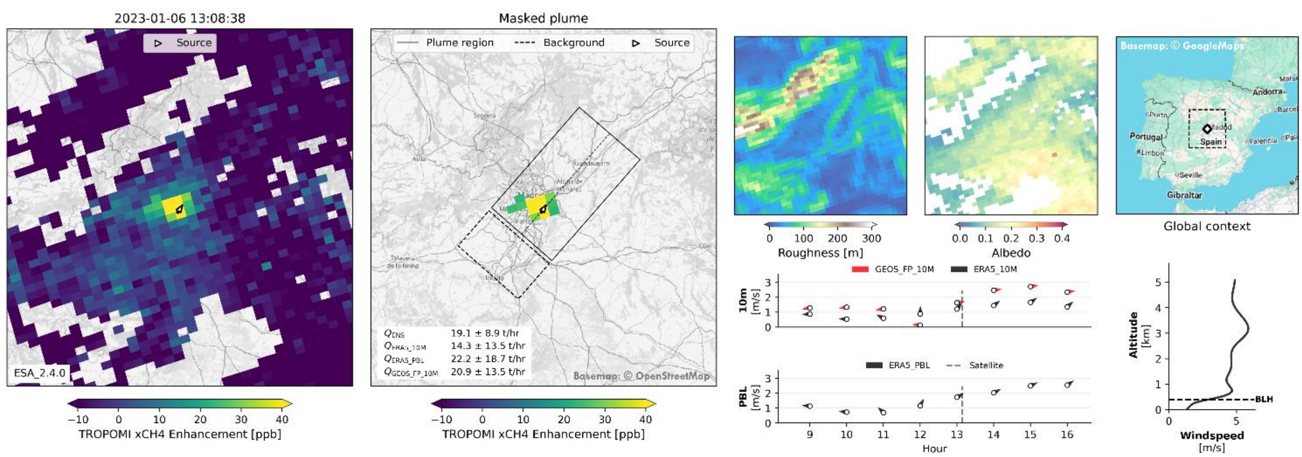

Figure 2: Example TROPOMI CH_4 plume showing the CH4 enhancement (left) the isolated plume with upwind-downwind box (centre), the surface roughness and albedo (top right) and the wind timeseries and vertical profile (bottom right).

https://doi.org/10.5194/egusphere-2026-3797
Preprint. Discussion started: 31 August 2026

3.2.2 GHGSat

The Canadian company GHGSat operates a satellite constellation of 13 methane-sensitive Fabry-Perot spectrometers which perform targeted observations of individual facilities at high spatial resolution (25 x 25 m^2) over small areas (10 x 15 km^2, Jervis et al, 2021). Emissions were quantified using the IME method, with modifications detailed in section 4.3.2. GHGSat reports a point-source detection limit of ~100 kg/hr under ideal conditions (Sherwin et al., 2023). For more diffuse sources like landfills, the detection limit is likely higher (Maasakkers et al., 2022). The dataset presented here contains ~200 CH_4 plumes from facilities near Madrid between August 2021- July 2024. In a few cases, multiple plumes were observed from the same site within the same overpass. For simplicity, site specific emission rates from same-day, same-observation-time plumes were summed, but emission rates for same-day, different-observation-time plumes were maintained as unique emission rates.

3.2.3 GHGSat Aircraft Observation (GHGSat-AV)

In addition to satellite observations, an aircraft was fitted with a modified GHGSat spectrometer, capable of 1 m resolution observations. GHGSat-AV on this platform has a quoted detection limit of ~10 kg hr^{-1} for an individual plume under ideal conditions, confirmed via controlled release (El Abbadi et al., 2024). Aircraft plumes were quantified using the Cross-Sectional Flux method. Flights were performed over the landfills for two consecutive days (01-07-2022 and 02-07-2022) under light winds (1.5 – 3 m/s). Flight lines were overlapped slightly to ensure complete coverage, which occasionally resulted in two observations of the same plume within this overlap region. Emissions were therefore averaged for any two sources detected within 10m of a source from a previous flight line.

3.3 Multispectral Imagery

Multispectral imagery from Sentinel-2 was used to independently identify active and inactive cells of the landfills, so that methane plumes could be related to landfill operation (methane enhancements were not retrieved from these observations). Sentinel-2 13-band imagery was used in combination with a change detection approach, similar in method to Dogniaux et al. (2025), but with modifications outlined in the supplement to account for parallax distortion of raised landfill cells with variable viewing geometry. The output of this was a geolocated spatio-temporal log of activity for each landfill.

3.4 Pollutant Release & Transfer Register (PRTR)

The European Pollutant Transfer and Release Register (E-PRTR) is a public database designed to increase the transparency and accountability of emissions by requiring industrial emitters to report annual emission statistics. It supports the Industrial Emissions Directive (IED), providing a mechanism to collate and evaluate emission performance from facility to national levels, using standardised and approved techniques across all nations. Facilities generally self-report, but their reported emissions have to be derived using standardised and approved methodologies which are then verified and approved by the national regulator (e.g., for Spain: Ministry for Ecological Transition and the Demographic Challenge, MITECO) before

https://doi.org/10.5194/egusphere-2026-3797
Preprint. Discussion started: 31 August 2026

being added to the E-PRTR. Most sectors, including waste management, use bottom-up activity-based emission calculations for their emission reporting, due to difficulties in directly measuring whole-site emissions. For landfills, this is typically a combination of emission factors based on waste influx, composition, active area, decay rates, and gas capture efficiency (if gas capture is installed). The used version of the E-PRTR (v18) contains data from 2006 – 2022. The E-PRTR is due to be replaced by the Industrial Emissions Portal Regulation (IEPR), with the first report due in 2028. The E-PRTR is unlikely to be updated before then, but PRTR-España continued to report this information nationally for MITECO, with data available for 2002 – 2024.

3.5 Gridded emission inventories

Two gridded emission inventories were used for additional comparison to satellite-based emission estimates; The Copernicus Atmosphere Monitoring Service regional inventory (CAMS-REG) and the Emissions Database for Global Atmospheric Research (EDGAR). CAMS-REG and EDGAR were analysed between 2008-2022 at a gridded resolution of 0.05 x 0.1° for CAMS-REG and 0.1 x 0.1° for EDGAR. To compensate for population and facility proxy-based scaling, we compare the total emissions for the Community of Madrid, rather than the nearest grid cell, making this more suitable for comparisons to TROPOMI-based estimates.

3.6 Meteorological data

Modelled meteorological information was acquired from ERA-5 (0.25° x 0.25°, Hersbach et al., 2020) and GEOS-FP (0.25° x 0.3125°, Molod et al., 2012). Both products provided 10 m winds from the single-level products. Planetary Boundary Layer winds were calculated from ERA-5 on pressure levels, taking a pressure-weighted average wind speed between the surface and the boundary layer height. Parameters were interpolated spatially to the satellite swath and temporally to the overpass time. In situ wind information was acquired from local air quality monitoring stations, namely Rivas-Vaciamadrid (station. 28123002) for Las Dehesas, and Valmodero (station. 28161001) for Pinto.

https://doi.org/10.5194/egusphere-2026-3797
Preprint. Discussion started: 31 August 2026

4 Results

4.1 Reported emission rates

Both CAMS-REG and EDGAR indicate that solid waste and wastewater management are the predominant source of CH_4 in the region of Madrid, accounting for 72 and 80 % of estimated emissions respectively, with both placing the majority of emissions within the grid cells containing the two landfills, weighted slightly more to Pinto than Las Dehesas (Figure 3). EDGAR regards landfill and wastewater categories separately, of which they account for 64% and 16.6% respectively. Total Madrid emissions were moderately stable across 2008 – 2022, averaging 8.44 ± 0.63 t/hr for CAMS and 7.54 ± 0.42 t/hr for EDGAR (mean ± σ).

The E-PRTR only contains emission information for Las Dehesas, Pinto, and a handful of smaller emission landfills. No other potential sources, such as the nearby WWTPs, exceed the operational capacity thresholds that would require them to report their emissions of CH_4. Figure 4 shows reported E-PRTR emission rates from Pinto and Las Dehesas for 2002 – 2024.

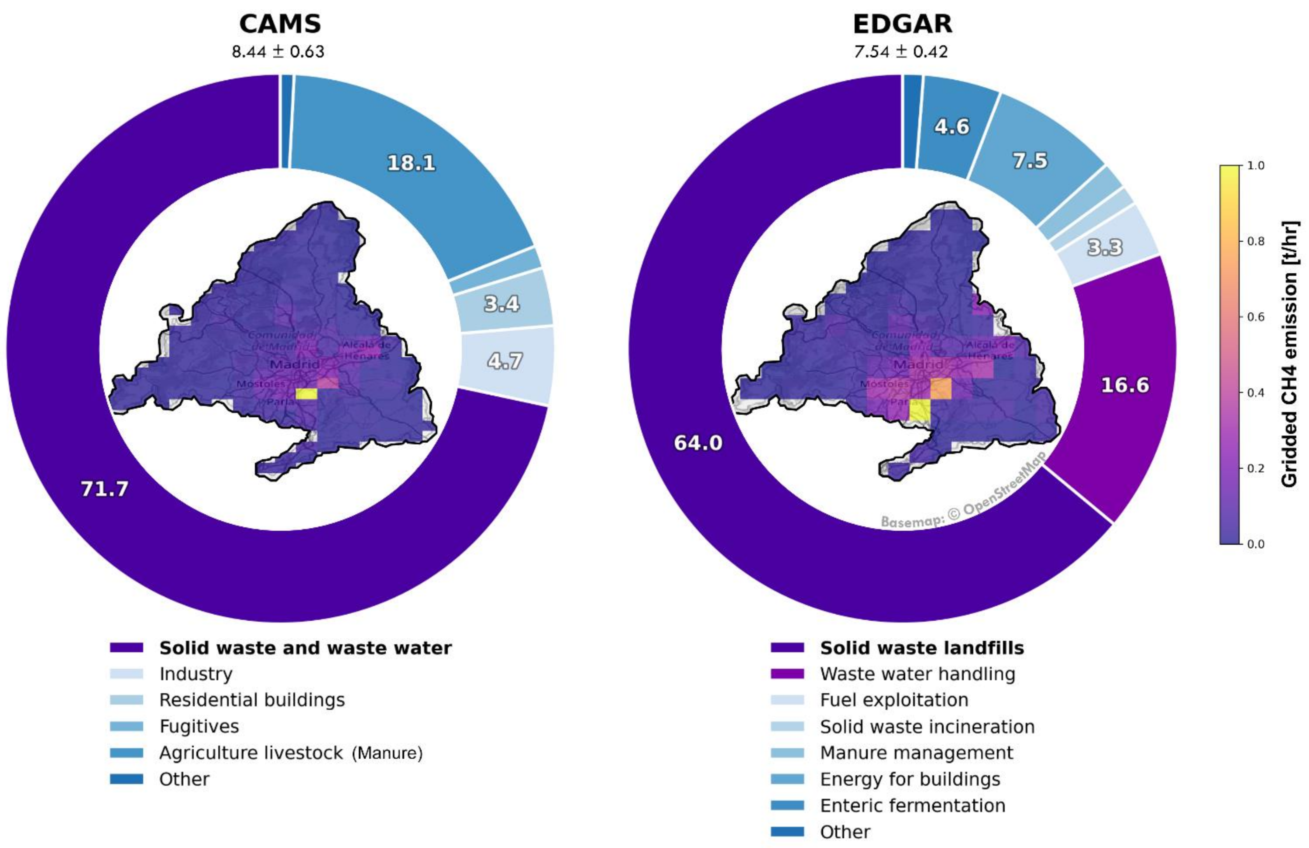

Figure 3: CAMS and EDGAR CH_4 emission inventories for 2022 for the Community of Madrid, Spain. Annual average (2008-2022) quoted as mean ± σ.

https://doi.org/10.5194/egusphere-2026-3797
Preprint. Discussion started: 31 August 2026

Emissions were comparable between the sites from 2002-2016, with Las Dehesas fractionally larger until 2014. Pinto's reported emissions exceed Las Dehesas from 2014 onwards, and consistently increased from 0.64 t/hr in 2012 to 1.55 t/hr in 2021. Pinto reported a 97.6% drop in emissions between 2021-2022, which coincided with a change from a calculated (C) to a measured (M) approach, in this case these were electrochemical cell measurements. These type of insitu measurements are valuable to detecting individual leaks, but are known to be insufficient for capturing whole site diffuse emission and typically cannot be performed on the active cell (Mønster et al., 2019). Las Dehesas reported emissions fluctuated between 0.8 – 1.0 t/hr until 2020, where reported emissions dropped 69% from 0.94 t/hr in 2019 to 0.29 t/hr in 2020, and have remained low between 0.17 - 0.32. Las Dehesas emissions in the E-PRTR have been calculated (C) since 2005, using emission factors from the Methodological Guide for the Development of Emission Inventories (Regional Government of Andalusia). All methods used for PRTR reporting are standardised approved methodologies designed to ensure consistency and comparability across facilities and EU Member States. These estimates are typically based on emission factors and activity data, and therefore may not fully capture short-term variability caused by operational or meteorological conditions.

Figure 4 also shows total waste tonnage entering Las Dehesas and Pinto landfill, separated by waste type. Facility-level waste data for both sites was obtained from the MITECO "*Annual report on the generation and management of municipal waste*" reports for 2018-2023 (MITECO, 2023). Annual values are reported by individual facilities, submitted to the regional government for validation, and compiled nationally by MITECO. The dataset records input and output tonnage of waste for every waste treatment facility in Spain, including MBT treatment facilities, waste to energy installations, and landfills. "Raw" waste includes mixed municipal waste, biodegradable waste from parks and gardens and wastewater treatment plant sludge. "Treated rejects" includes all waste that has passed through a MBT facility before landfill that could not be recovered for recycling, composting, or energy. Pinto handles a larger amount of waste than Las Dehesas, with 602 kt of waste accepted at Pinto and 473 kt accepted at Las Dehesas in 2023. Pinto had an average raw waste fraction in 2018 of 88% compared to 38% for Las Dehesas, which then reduced to 75% and 5% respectively in 2023. In recent years Las Dehesas waste fractions have become predominantly rejected waste from the various MBT facilities at Valdemingomez Technology Park, whereas Pinto sends a large fraction of raw, untreated municipal waste directly to landfill, as shown in Figure A. 3.

Reductions in reported CH_4 emissions can be due to a range of factors including the completion of cells, final capping, improvements to gas extraction efficiency, gas utilisation, improved landfill design, aging landfill cells, and changes to waste volume/composition received. Large, sudden changes are typically related to changes in reporting methodologies, activity scaling factors, or measurement methods, rather than physical on-site changes. The transition in waste composition at Las Dehesas may partly explain the reduction in their reported emissions. However, the justification for such a stark reduction in reported emissions from both facilities is currently not clear from the reporting alone. All values discussed here are reported publicly via E-PRTR, PRTR-España, and MITECO.

https://doi.org/10.5194/egusphere-2026-3797
Preprint. Discussion started: 31 August 2026

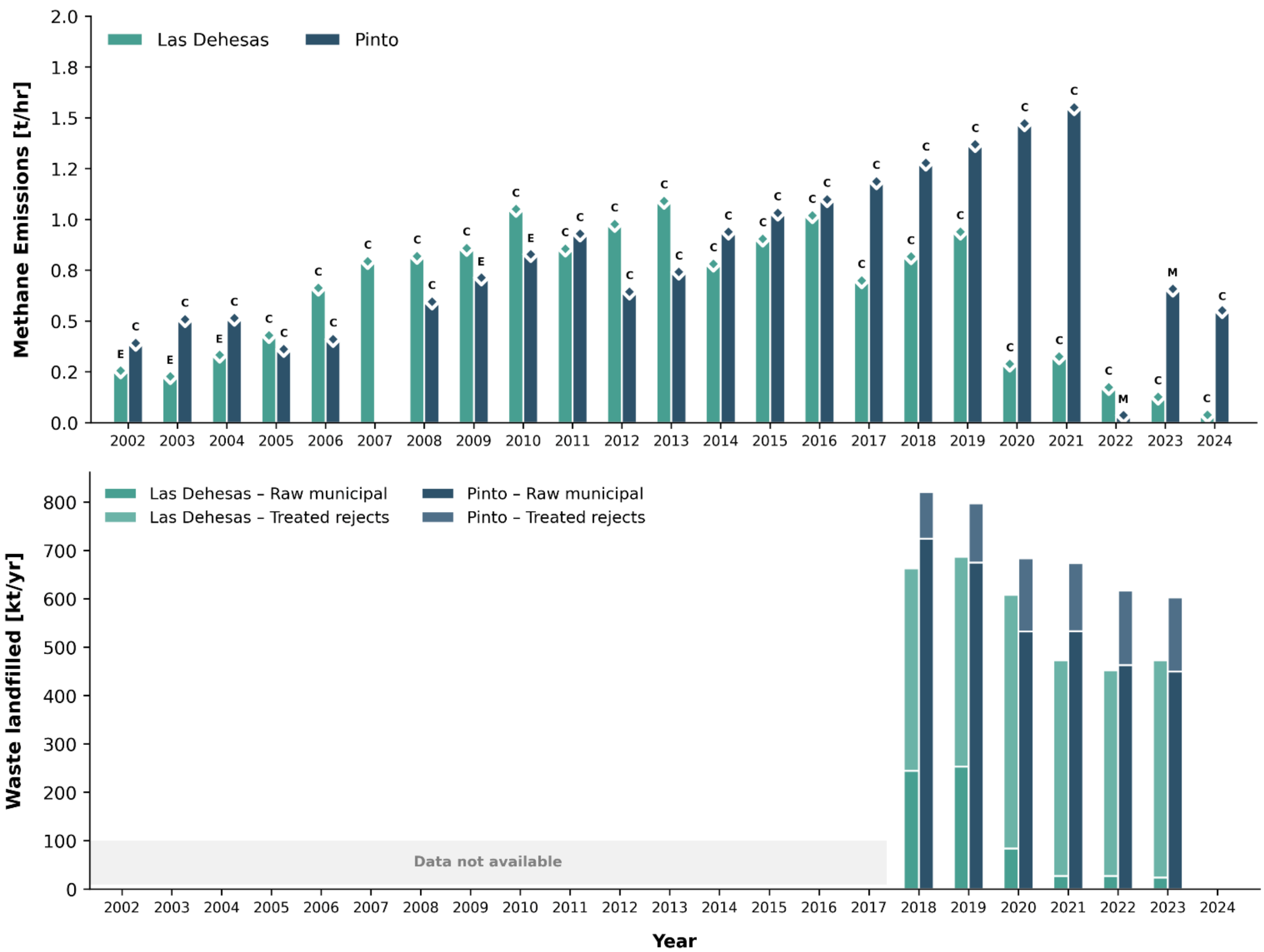

Figure 4: PRTR-Espana reported CH₄ emissions (top) and waste landfilled (bottom). Data available at prtr-es.miteco.gob.es/ and miteco.gob.es/ respectfully, provided by MITECO. Letter annotations refer to Estimated (E), Calculated (C), or Measured (M).

https://doi.org/10.5194/egusphere-2026-3797
Preprint. Discussion started: 31 August 2026

4.2 TROPOMI Enhancement

Figure 5 shows seasonally and annually averaged CH_4 enhancements derived from the ESA Operational v.2.4.0 data product, where each daily enhancement was found by subtracting the average $XCH_4 \pm 1°$ (~85 x 85 km) around the centre of Madrid, resampled onto a ~1km regular grid. The equivalent figure for the IUP-UB WFMD TROPOMI product is given in Figure A. 4. Days with less than 30% coverage were omitted from the average. For all years (2018-2024) there was a strong and distinct enhancement of CH_4 above the city of Madrid, biased towards the two landfills and away from the city centre. This localized enhancement above Madrid was a persistent feature across the whole TROPOMI observation record, varying slightly year-on-year with a clear increase in intensity towards 2023-2024 in both data products, though this could be due to

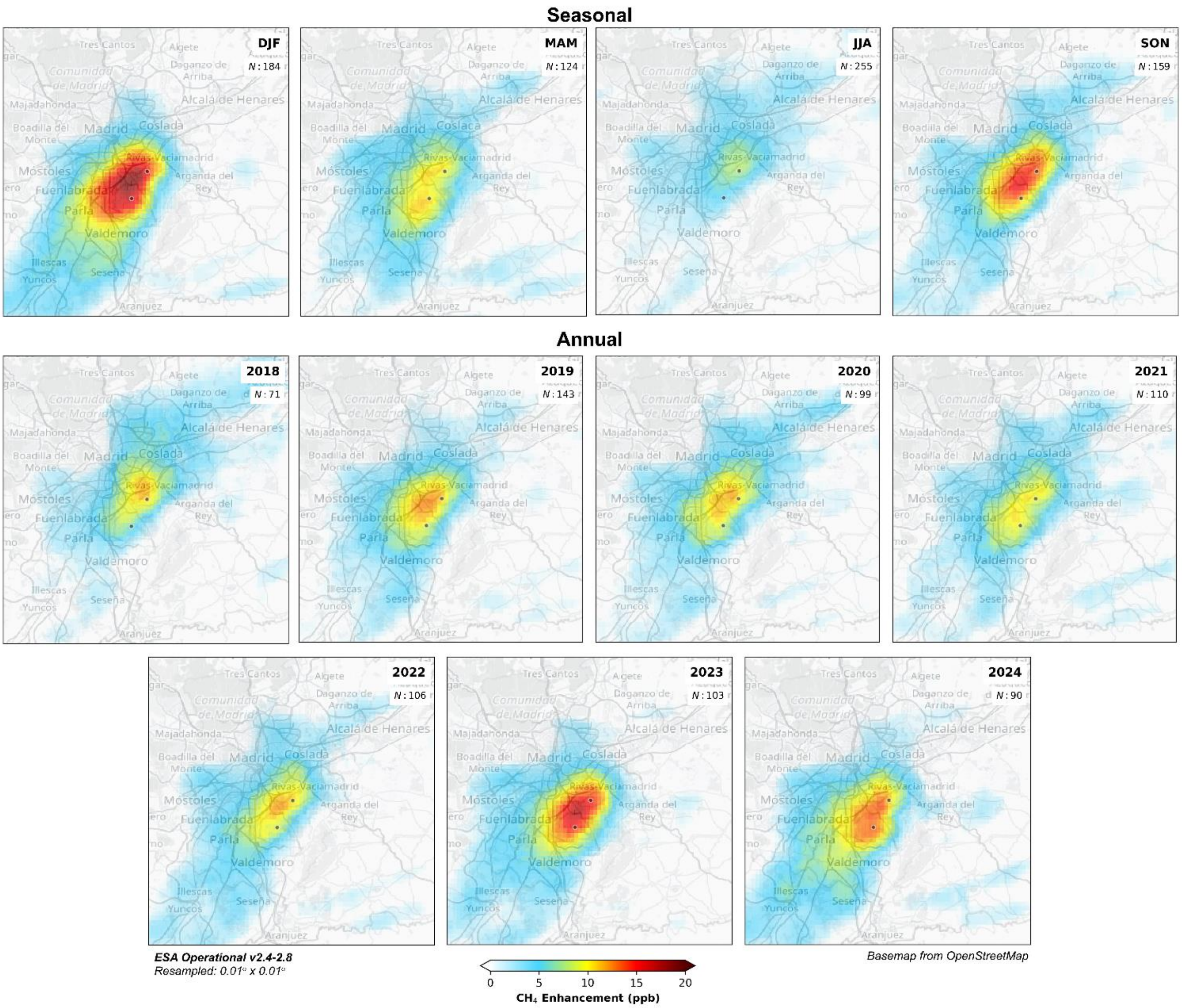

Figure 5: Seasonally (top row) and annually averaged CH_4 enhancement from the Sentinel-5P ESA XCH4 v2.4.0 product for years 2018-2024, where days with < 30% coverage of the domain were omitted.

https://doi.org/10.5194/egusphere-2026-3797
Preprint. Discussion started: 31 August 2026

sampling differences. There was a strong seasonal variation to the observed enhancement, with peak enhancements over autumn-winter, and lower enhancement over summer. This is likely associated with meteorological effects such as a shallower PBL and reduced dispersion in wintertime, leading to greater localised accumulation of CH_4 in winter. This seasonal trend may also be related to seasonal variability in landfill emissions (Rachor et al., 2013).

4.3 Estimated emission rates

4.3.1 TROPOMI

For the entire 2018-2024 TROPOMI data record, observed emissions from Madrid averaged 11.8 ± 8.7 t/hr (IUP_{SB}, 215 plumes), 12.4 ± 8.8 t/hr (ESA_{SB}, 213 plumes), and 14.9 ± 10.0 t/hr (ESA_{ML}, 222 plumes). Annual and total averages are given in Table 1. Emission estimates based on the IUP product were slightly lower than both ESA estimates, regardless of the method. Both statistics-based methods yielded lower emission estimates on average compared to the machine learning approach, likely due to slight differences in background estimation, wind retrieval, and plume masking, with the ML approach often including more pixels in the plume mask compared to the SB method. In addition, plumes unique to the SB methods tended to be lower emission plumes, whereas plumes unique to the ML method had a range of small to large plumes (Figure A. 6). Emission rates were highly correlated between ESA_{SB}, ESA_{ML}, and IUP_{SB} ($R = 0.84$-0.91), showing consistency despite fundamental differences in the approach. For the SB methods there were 46 plumes unique to IUP_{SB} compared to 44 unique to ESA_{SB}, representing around 20% of each dataset (Figure A. 6). This highlights the value of simultaneously processing both data products, yielding greater coverage of the region. Emission rates were fairly stable on average regardless of the wind product used, with a slight high bias in the emissions quantified using the PBL winds (Figure A. 7), despite using a PBL-specific effective wind (U_{eff}) calibration (Schuit et al., 2023). All approaches rely on a clear identifiable plume, and therefore

Annual Mean Emission Rate (Emission rate [t/hr])

Year	ESA_{SB}	IUP_{SB}	ESA_{ML}
2018	12.3 ±6.6	12.0 ±7.9	14.4 ±7.4
2019	11.1 ±6.6	9.9 ±4.5	12.3 ±6.9
2020	12.3 ±8.6	11.1 ±6.8	17.5 ±11.3
2021	13.0 ±8.3	12.7 ±8.8	13.6 ±9.7
2022	15.4 ±13.2	13.4 ±10.5	16.1 ±9.7
2023	12.2 ±8.9	13.1 ±11.7	16.2 ±12.8
2024	11.2 ±8.5	10.4 ±7.3	14.1 ±8.5
All Years	12.4 ±8.8	11.8 ±8.7	14.9 ±10.0

Annual plume count (Number or plumes)

Year	ESA_{SB}	IUP_{SB}	ESA_{ML}
2018	18	14	16
2019	36	38	39
2020	34	28	30
2021	28	26	24
2022	27	29	32
2023	44	47	47
2024	26	33	34
All Years	213	215	222

Table 1: TROPOMI derived CH_4 emissions (left) and plume counts (right) for ESA_{SB}, ESA_{ML} and IUP_{SB} processing approaches.

https://doi.org/10.5194/egusphere-2026-3797
Preprint. Discussion started: 31 August 2026

do not account for weaker plumes or non-detects. The detection limit of TROPOMI is often quoted as ~4 t/hr in Jacob et al. (2016), 0.5 – 8 t/hr in Dubey et al. (2023) and 8 t/hr in Schuit et al., 2023 (5th percentile of the detected emission rates), depending on wind conditions and source type. Emission rates based only on detected plumes may represent the upper bound of emissions, as smaller but valid emissions around or below the detection limit are not included in the average (Dogniaux et al., 2025). Using an ensemble of winds from local met stations within 30km of the landfills led to averages from 8.6 to 11.4 t/hr across methods, with reduced peak rates of 30 t/hr maximum. However, as we only have in situ data from 2020 onwards, this has not been applied to the full dataset. Emission rate distributions for all methods and wind products are shown in Figure A. 7, which highlights the choice of meteorological product as the main contributor to variability with only slight differences between processing method and XCH_4 data product.

4.3.2 GHGSat

The GHGSat dataset consisted of 111 observations with a total of 109 plumes for Las Dehesas and 107 for Pinto. Average emissions for the entire timeseries were 2.4 ± 1.3 t/hr for Las Dehesas and 3.7 ± 2.0 t/hr for Pinto with peaks of 4.4

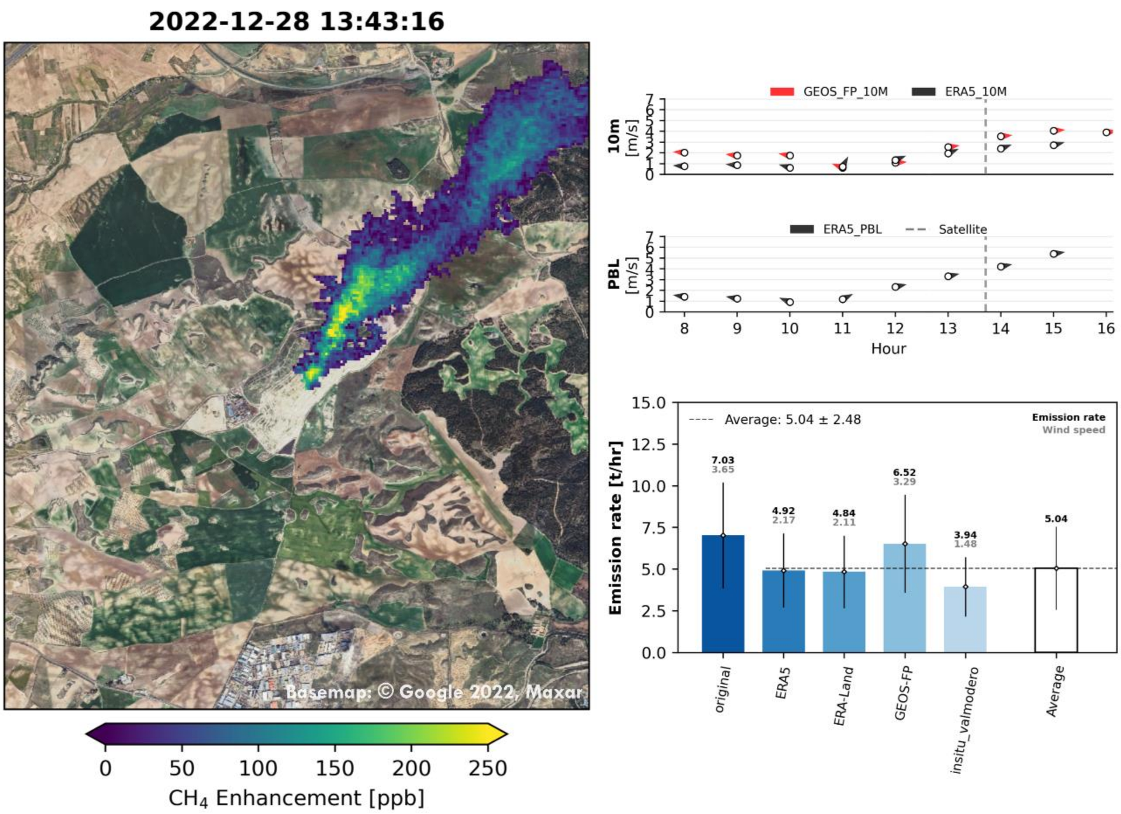

Figure 6: CH_4 plume observed by GHGSat from Pinto Landfill, Madrid, on the 28th December 2022 (left), with wind parcel history from ERA5 and GEOS-FP (upper right) and recalculated emissions using various meteorological products (lower right).

https://doi.org/10.5194/egusphere-2026-3797
Preprint. Discussion started: 31 August 2026

t/hr and 7.0 t/hr respectively (95th percentile), using emission rates derived by GHGSat. GHGSat used a combination of GEOS-FP and OpenWeather for their wind information, and used a point source calibration. There were no available wind measurements on-site. The IME method is highly sensitive to the magnitude of the wind and wind speeds derived from different wind products can vary considerably day-to-day. Emission rates were therefore recalculated using ERA5 10 m, ERA-Land 10 m, GEOS-FP 10 m, and the nearest local monitoring station to each landfill, in an attempt to minimise variability introduced by the representativeness of each individual wind field (Figure A. 8). Figure 6 shows a typical GHGSat observation over Pinto, alongside wind history from either side of the satellite overpass and the recalculated emission rates based on each wind product. GEOS-FP gave a consistently larger wind speed than both ERA5 and the in-situ monitoring station, potentially due to its coarser resolution in this semi-mountainous region (Figure A. 4). Rates were also recalculated using the area U_{eff} calibration from Maasakkers et al. (2022), resulting in a final average emission estimate of 2.5 ± 1.3 t/hr for Las Dehesas and 3.8 ± 2.0 t/hr for Pinto using the ensemble wind and area U_{eff} calibration, with peaks of 3.6 t/hr and 5.2 t/hr respectfully (95th percentile).

In addition to the two landfills, emissions were also detected at the E.D.A.R. Sur WWTP, located to the south west of Las Dehesas. There was a total of 19 plumes detected from E.D.A.R. Sur with a mean rate of 0.5 t/hr, peaking at 1.1 t/hr (Figure A. 9). These plumes originated from the north end of the facility where there appears to be digestion and gas storage tanks. There was a single moderate plume detected from the biogas upgrading facility (PTB) at the north east end of the VTP with an emission rate of 1.1 t/hr (Figure A. 10). The low frequency of detection from the PTB implies a transient emission source e.g., maintenance, rather than a persistent leak. Neither facility currently exceeds the operational activity capacity or estimated emission thresholds that would require them to report emissions to the E-PRTR.

4.4 GHGSat-AV

Aircraft-derived total site emission averaged 3.0 ± 1.8 t/hr for Las Dehesas and 4.6 ± 2.7 for Pinto, based on two observations from 2022-07-01 and 2022-07-02. Measurements were taken between 11:17 – 12:06 for 2022-07-01 and 08:51 – 09:54 for 2022-07-02, with wind speeds averaging 0.9 and 2.8 m/s respectfully. There was a same-day GHGSat observation on the 2022-07-01 for each site. GHGSat emissions on this day were in good agreement, albeit slightly higher within uncertainty ranges than GHGSat-AV for Las Dehesas (+ 0.5 t/hr) and slightly lower for Pinto (- 0.3 t/hr), using the area-calibrated ensemble wind (Table 2). The airborne measurements were approximately 1.5 hours after the satellite overpass. Krautwurst et al. (2025) performed an independent flight campaign over both landfills on the 4th August 2022 and found a combined emission rate 12.7 ± 3.4 t/hr using down-wind CSF, compared to an average combined-site rate of 7.6 ± 4.5 t/hr from GHGSat-AV using per-plume CSF. As Krautwurst et al. (2025) evaluates the whole down-wind plume rather than relying on individual sub plume masking, GHGSat-AV may be missing diffuse components of the emission, leading to an apparent underestimation. They also consider impact of additional contributing sources, with a worst-case impact of 2 t/hr based on all nearby non-landfill contributing sources reported in EDGAR v8.0. Krautwurst et al. (2025) quote a per flight line 1σ of up to ~5 t/hr, implying that local per-observation turbulence can heavily influence the derived emission rate, and multiple

https://doi.org/10.5194/egusphere-2026-3797
Preprint. Discussion started: 31 August 2026

independent flight lines across multiple days would be needed to minimise this effect. As we do not have coincident GHGSat and GHGSat-AV measurements on the 2nd July, we cannot separate real emission variability from differences in wind speed, observation time, and instantaneous turbulence between observations. This is discussed further in Section 4.7.

		Las Dehesas		Pinto		Combined total	
Source	**Date**	**Emission rate [t/hr]**	**Uncertainty [t/hr]**	**Emission rate [t/hr]**	**Uncertainty [t/hr]**	**Emission rate [t/hr]**	**Uncertainty [t/hr]**
GHGSat	01/07/2022	2.1	1.2	2.2	1.2	4.3	1.7
Aircraft	01/07/2022	1.6	0.9	2.5	1.5	4.1	2.4
	02/07/2022	4.4	2.6	6.6	3.9	11.0	6.5
	2-Day average	3.0	1.8	4.6	2.7	7.6	4.5

Table 2: GHGSat-AV total site emission rates compared to GHGSat satellite

4.5 Intercomparison of emission rates

Figure 7 compares emission rates from all previously described approaches and data sources, as well as emission rates for Madrid from the literature. Top-down derived emission rates (satellite, aircraft) were substantially higher than bottom-up emission rates (CAMS, EDGAR, E-PRTR) for both regional and facility scale comparisons. CAMS and EDGAR were similar (between 7.5 – 8.5 t/hr) and therefore averaged for simplicity. Average TROPOMI emission rates were ~60% larger than estimated in CAMS or EDGAR when comparing the whole Madrid region though this must be considered in the context of TROPOMI's plume detection limit and sensitivity, with TROPOMI likely sampling the upper end of emission rates. For example, Dogniaux et al (2025) showed plume-based IME average emission rates were biased high compared to inversion-based emission rates for the same urban source, as the inversion can include emission days below the plume detection threshold. GHGSat and GHGSat-AV emissions were 4.6 – 5.2 times larger respectively compared to average facility E-PRTR reported emissions. Even when considering pre-reduction E-PRTR emission rates (2018 - 2021), GHGSat and GHGSat-AV were still 3.2 – 3.8 times larger than reported. These results are broadly consistent with other studies of these landfills, namely; Dogniaux et al (2025), Krautwurst et al (2025) and Tu et al (2022a), even considering the differences in methodology, data processing, and timeframe. GHGSat combined emissions did compare well to total regional CAMS and EDGAR waste sector emissions, with the inventories averaging ~6.1 t/hr for the waste sector, though this comparison breaks down when considering the landfill containing grid cells only, with Las Dehesas and Pinto containing cells approx. 0.38 and 1.62 t/hr respectfully in CAMS and 0.74 t/hr and 1.64 t/hr in EDGAR for 2022. Therefore, comparison between GHGSat and the regional inventory are probably not suitable. TROPOMI-derived emissions were greater than GHGSat combined emissions from both landfills, which is to be expected as TROPOMI-scale plumes will include emissions from all sources in Madrid e.g., wastewater and more diffuse

https://doi.org/10.5194/egusphere-2026-3797
Preprint. Discussion started: 31 August 2026

emissions. Neither TROPOMI nor GHGSat show a significant change in emissions in 2022-2024, despite the reported drop in the E-PRTR for both facilities.

Peak observed emission values occurred in the first half of January 2023, at both the regional scale (TROPOMI), but crucially also at the site-specific scale (GHGSat), indicating that the landfills drove this spike in emissions. January-February 2023 saw the largest emission rates from both individual sites with GHGSat, with emissions peaking at 7.15 t/hr for Las Dehesas and 10.83 t/hr for Pinto respectively, and with regional emissions in excess of 40 t/hr from TROPOMI. It is unclear what drove this peak in observed emissions. Initial inspection of Sentinel-2 and Planet imagery do not indicate any large-scale operational changes at either site. We cannot rule out greater emissions on non-observed days.

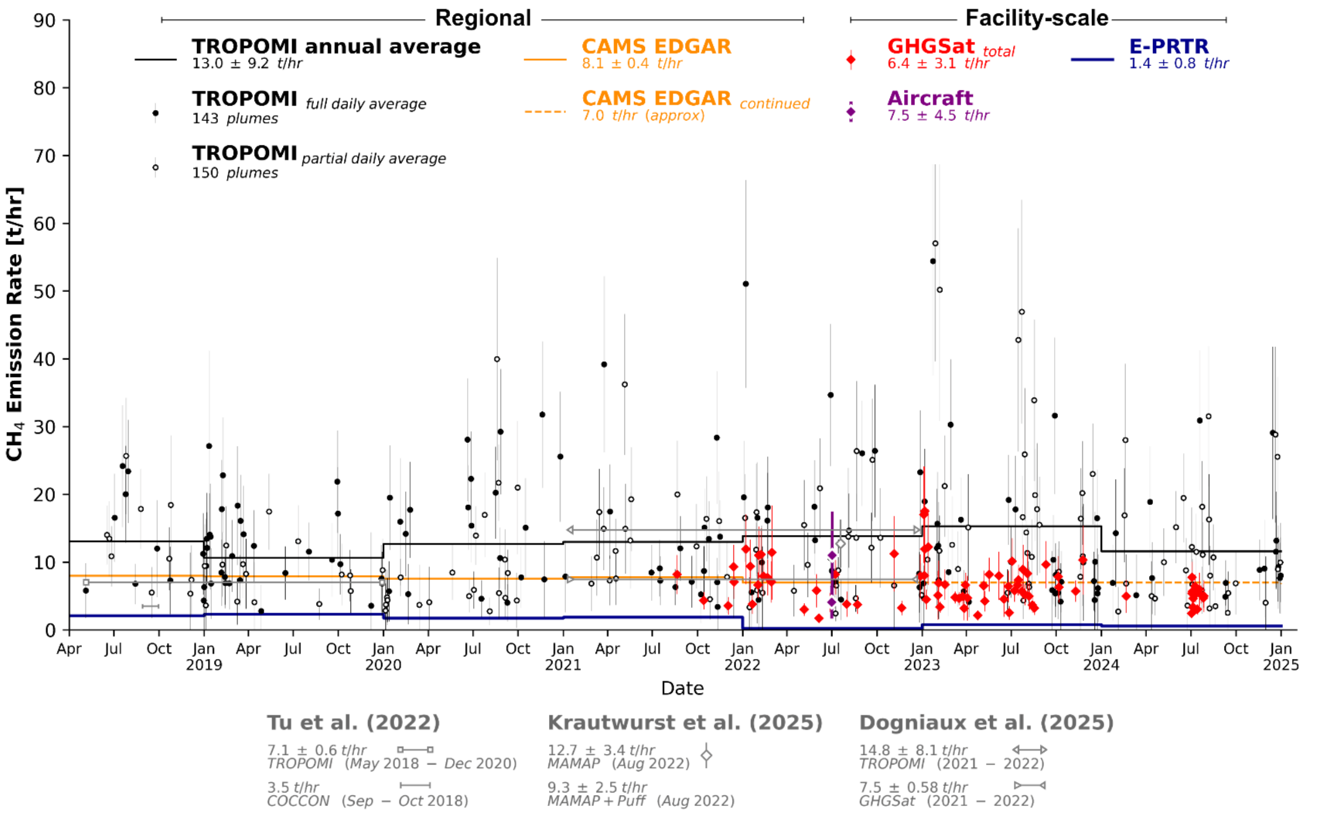

Figure 7: Emission rates calculated for Madrid (TROPOMI, CAMS, EDGAR), and combined totals for the landfills (GHGSat, GHGSat-AV, E-PRTR), with values quoted as mean ± σ. Due to similarity and consistency of estimates, CAMS and EDGAR emission rates have been averaged, and also extended beyond 2022 indicatively. TROPOMI estimates represent the average of the three methods (ESA_{SB}, ESA_{ML} and IUP_{SB}), as a "full average" when all methods have a plume, and "partial" when only 1-2 methods have a plume.

https://doi.org/10.5194/egusphere-2026-3797
Preprint. Discussion started: 31 August 2026

4.6 Interpreting the origin of GHGSat observed plumes

Sentinel-2 imagery was processed for a 5-year period (2020-2024), during which time each landfill constructed, filled, and capped multiple cells. Figure 8 shows Sentinel-2 detected surface changes at each landfill and estimated GHGSat CH_4 plume origins, both coloured by time-of-measurement. GHGSat observations were filtered to those with clear, identifiable "origin" points, omitting ~25% of observations for each landfill. GHGSat sampling density was best for 2023 with 38-44 filtered observations, and was lower for 2021/22/24 with between 5-20 observations.

Las Dehesas showed activity across its active cells at the southern end of the facility. Activity in 2021 was focused on LD-2, as the cell neared the end of its construction. LD-2 was completed in 2022 and LD-3 became the working cell towards the end of 2022. Activity since 2023 has been entirely within LD-3, moving with the working face around the active cell.

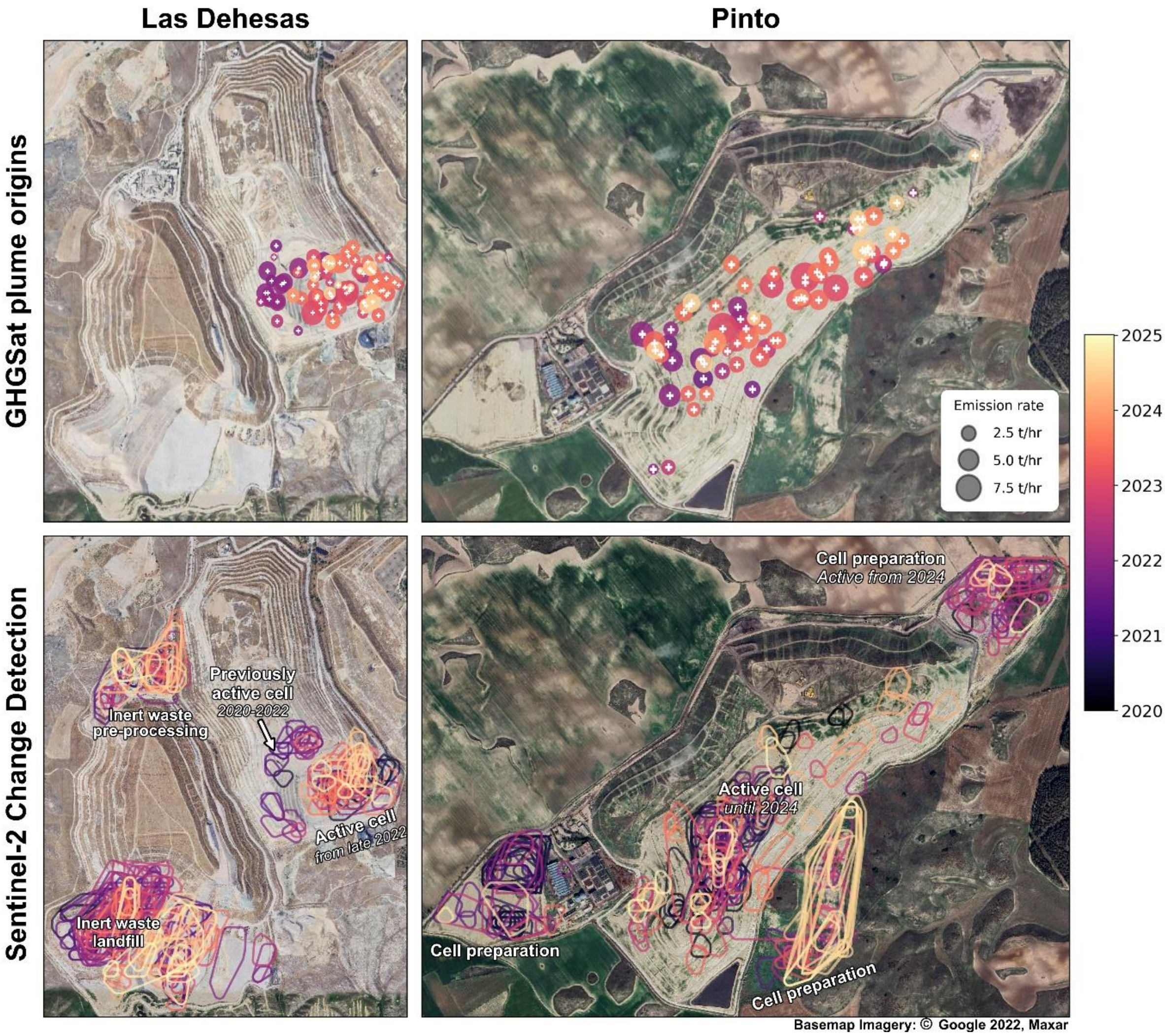

Figure 8: Comparisons between Sentinel-2 change detection to the estimated origins of GHGSat CH_4 plumes for the 2021-2025 time period

https://doi.org/10.5194/egusphere-2026-3797
Preprint. Discussion started: 31 August 2026

Landfill	Region	Status	% of annual plumes [Number of plumes per year]			
			2021 [5]	**2022 [20]**	**2023 [44]**	**2024 [10]**
Las Dehesas	LD-1	Capped	-	-	-	-
	LD-2	Active until 2022	80%	60%	11%	-
	LD-3	Active from 2022	20%	40%	89%	100%
			2021 [7]	**2022 [16]**	**2023 [38]**	**2024 [12]**
Pinto	P-1	Capped	-	6%	-	-
	P-2	Active	100%	94%	100%	92%
	P-3	Active	-	-	-	-
	P-4	Active	-	-	-	8%

Table 3: Percentage share of plume origin per landfill region per year for Las Dehesas and Pinto

GHGSat plumes originated predominantly from LD-2 in 2021-2022, during which time this was the active cell. As activity transferred to LD-3 so did the origins of the observed GHGSat plumes. The share of GHGSat plumes attributed to LD-3 grew from 40% in 2022 to 100% in 2024, demonstrating the strong link between the active cell and the bulk of detected emissions. Activity was detected at La Salmedina processing facility (LS-1) and active cell (LS-3) to the west of Las Dehesas, but as La Salmedina handles mostly construction waste, methane was not detected.

The right panels of Figure 8 show Pinto which had activity localized to three main areas, the central active cell (P-2) with two smaller cells to the east (P-3) and west (P-4). P-2 saw activity for the whole time period, from 2021-2025. P-2 was the primary active cell of Pinto for the whole period, completed mid-2024. Activity in P-3/P-4 appeared to be clearing and preparation work, rather than active deposition of waste. P-4 became the active cell at the end of 2024. GHGSat plume origins were highly correlated to the active cell, P-2, with up to 100% of plumes originating from this region, with little change between 2021-2024.

The correlation between CH_4 emission origin and site activity found here agrees well with recent on-site, aircraft, and satellite studies of global landfills, which found the majority of remotely-detected emissions can be assigned to the active cell (Cusworth et al., 2024; Dogniaux et al., 2025; Kumar et al., 2024; Maasakkers et al., 2022; Omidi et al., 2025; Scarpelli et al., 2024). Therefore, any approach to quantify emissions from these facilities needs to accurately describe emissions from the active cell. Failure to properly and completely account for these active cell emissions would lead to a major underestimation of the total site emissions. It should be noted that GHGSat origins are not exact and are estimated based on peak enhancement and wind direction. As a landfill is a heterogeneous source, the single origin point for the combined GHGSat plume could

https://doi.org/10.5194/egusphere-2026-3797
Preprint. Discussion started: 31 August 2026

represent the central weighted position of a combined multi-source emission. It does not rule out emissions from other regions, rather it only signifies where the *majority* of detectable emissions originate from.

The strong correlation between the active cell and the observed emission plume indicates that GHGSat is especially sensitive to the active cell due to both the magnitude of emission but also the spatially dense nature of this type of emission, acting closer to a point source. Beyond active face emissions and infrastructure leaks, methane is also expected to be emitted passively through the top cover of the whole landfill, and whilst a part of this may be oxidised (10 - 54%, IPCC-TFI, 2026; Chanton et al., 2009), a fraction will be emitted to the atmosphere. The enhancement per m^2 would be low, but cumulatively it could contribute significantly to the total site emission when scaled across the landfill, potentially 24 – 62 % of total emissions (Omidi et al., 2025). The sensitivity of the satellite and aircraft to the active cell, with the plume mask typically confined to within and immediately downwind of the active cell, implies that diffuse emission through the landfill top cover may not be fully captured by these remote methods, and may ultimately lead to an underestimation of the emission rate. To understand this further would require direct and coordinated downwind sampling of the total plume for comparison to the satellite.

4.7 Understanding the wind flip seen in Madrid and the impact on derived emissions

Madrid experiences a semi-frequent and strong diurnal wind flip centred around midday, crucially the same general time as most satellite overpasses, driven by diurnal mountain winds and the Iberian Thermal Low (ITL). The underlying meteorological and topographical factors behind this flip are explained in detail in A3. Figure 9 shows average ERA5 reanalysis 10m winds (top) and an averaged wind rose from a 14-station average of air quality monitoring stations across 2020-2024 (within 25 km radius of the landfills but not within the Madrid urban centre), both of which clearly demonstrate the wind flip. Figure 9 also shows the wind parcel history from ERA5 for all days in 2018-2024 separated by flip/no-flip (lower left), as well as just for days with detected TROPOMI plumes (lower right). Winds are predominantly northerly/easterly in the AM. Around 10:00, winds begin to shift, and by 13:00 onwards winds are majority southerly/south-westerly and stronger. This reversal in wind direction occurs throughout all months, though not every day, and the strength is lower in winter months (Figure A. 11). The onset is earlier in the day for summer months, and later in the day for winter months.

The impact of this wind flip was investigated by considering the maximum wind direction change (WDC) within a -4 to +1 hr window around that day's satellite overpass (typically 13:10 UTC for TROPOMI). Days with a maximum $\Delta\theta_{wind} >$ 120° within the overpass window were classed as flip days. There was a clear drop in wind speed observed during the onset of the flip, with winds at the time of overpass on flip days being ~1.6 m/s slower on average than non-flip days. Flips occurred on ~20% of all days between 2018-2024, but occurred on ~40% of days with positive TROPOMI plume detection. For all days (Figure 9, lower left), early morning winds averaged 1.8 m/s, which gradually increased from sunrise through to 15:00, reaching ~ 3 m/s at the time of TROPOMI overpass, where they then begin to decrease. When looking at the meteorology for days with positive TROPOMI plume detections (Figure 9, lower right), both flip and non-flip days experienced very similar morning wind speeds, where wind speed does not increase gradually from morning into the afternoon. It appears that a weaker

https://doi.org/10.5194/egusphere-2026-3797
Preprint. Discussion started: 31 August 2026

than average wind field provides the optimal conditions for plume detection from Madrid, regardless of the presence of a flip. Positive plume non-flip days experienced relatively stable and lower than average wind speeds throughout the day. Positive plume flip days saw a pronounced dip in wind speed during the flip between 10:00 – 13:00, which typically recovered by 15:00. The difference in wind speed between flip and no-flip days with positive plume detections ranges from 0.4 – 0.6 m/s on average. This happens to be common on flip days, hence the disproportionate number of flip days in the TROPOMI plume record (~40% compared to 20% for the whole time period). The flip has typically completed by the time of TROPOMI overpass. For TROPOMI derived emissions, we found a moderate difference in derived emission rates, with emissions derived on flip days between 2.7 – 3.7 t/hr lower than non-flip days on average, though this difference is not statistically significant across the majority of retrieval products ($p = 0.014–0.190$) and is well within the uncertainty of individual emission quantifications. The reduction in derived emission rates on flip days implies that the modelled wind may not accurately describe the dispersion experienced by the whole plume at TROPOMI scales, leading to an underestimation as a function of wind speed.

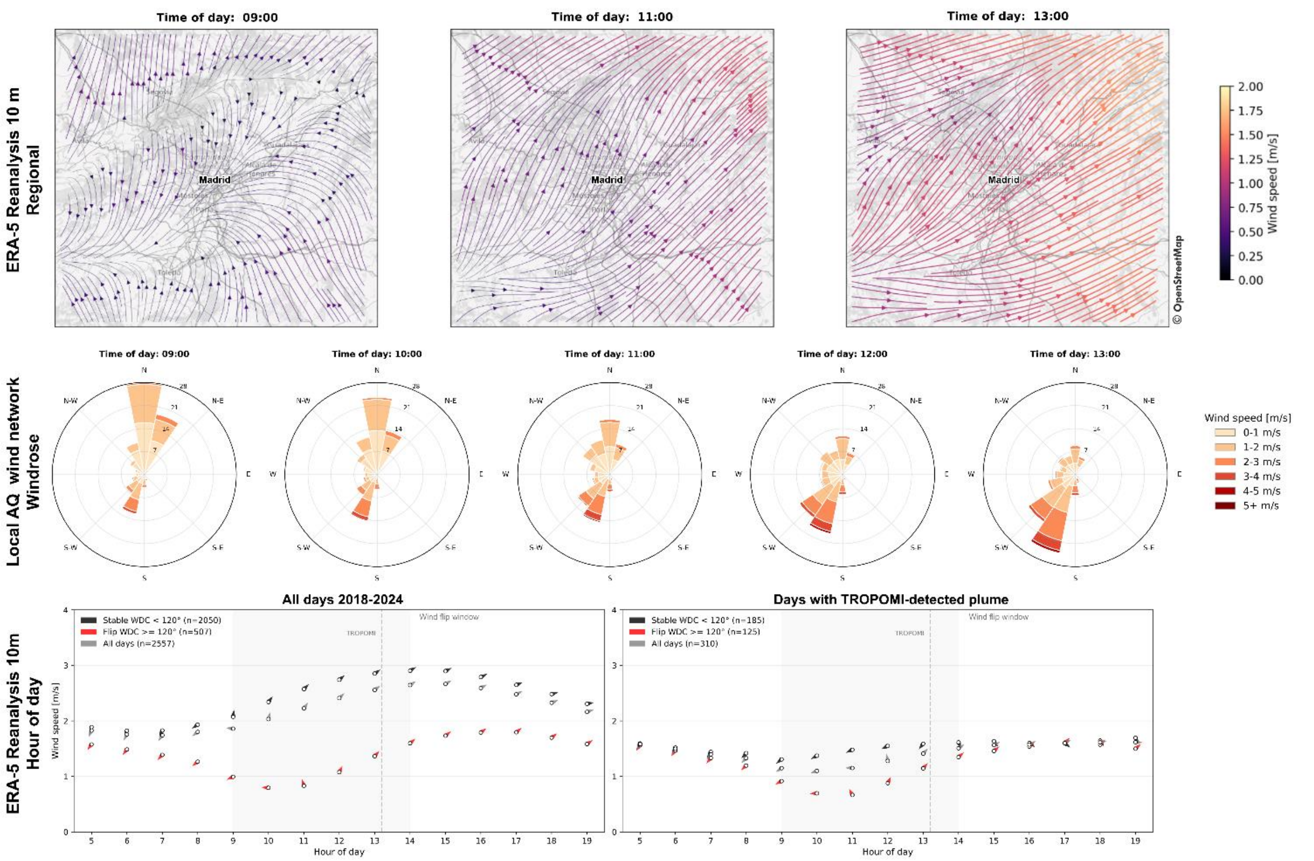

Figure 9: ERA5 reanalysis 10 m winds averaged 2020-2024 around Madrid for respective time of day (top), Rivas-Vaciamadrid air quality monitoring station average wind rose for respective time of day (middle), ERA-5 reanalysis average 10m wind speed and direction for all days (lower left) and for days with a TROPOMI-detected plume (lower right). All averages are over 2020-2024.

https://doi.org/10.5194/egusphere-2026-3797
Preprint. Discussion started: 31 August 2026

The reduction in derived emissions is well within the group standard deviation of 6 to 11 t/hr for flip and non-flip days respectfully. The coefficient of variation was slightly lower for flip days (0.55-0.57 compared to 0.69 – 0.77), indicating flip days are not proportionally more uncertain than non-flip days. We did not observe an emission reliance on flip days in GHGSat, likely due to GHGSat plumes being too short (approx. 0.2 – 1.5 km) to be influenced by multi-hour changes in wind direction. The timing of the flip may however describe the difference in aircraft-derived emission rates between the 1st and 2nd of July 2022, as the 1st July was measured at 12:00-13:00 local time on a flip day compared to 09:00 – 10:00 on a non-flip day. Whilst the flip may not impact the plume on these timescales, the validity of the modelled wind on these instantaneous plumes may be further decreased during flip conditions. In most cases, the flip has completed by the time of TROPOMI overpass, so whilst a flip is typically not in progress during the measurement, the plume morphology will have likely been impacted to a varying degree. Similar characteristic changes in meteorology can happen under various conditions, e.g., a methane source experiencing diurnal coastal winds, and therefore the impact of variable wind fields should be considered for per location. Care should be taken when interpreting individual day TROPOMI observations under dynamic/changing wind conditions.

5 Conclusion

This study presents the first dedicated long-term analysis of CH_4 emissions over Madrid using a combination of TROPOMI, GHGSat and GHGSat-AV measurements, and puts these emissions in the context of reported emissions. Top-down derived emission rates compared well but were consistently above bottom-up reported annual emissions in all cases, with regional scale plume-based top-down estimates (TROPOMI) 60% larger than regional inventories, and facility-scale top-down estimates (GHGSat, GHGSat-AV) between 3.2 – 5.2 times larger than reported emissions. This builds upon the growing collection of studies that have identified inconsistencies between satellite and reported emissions across multiple sectors, and whilst the magnitude of these differences varies, it suggests that the approved and standardised procedures used to generate these emission estimates may need to be re-evaluated more broadly. Top-down emission rates were remarkably consistent across the measurement time frame with little annual variation and no discernible long-term trend, despite moderate day-to-day variation. We showed how different evaluation of the same satellite products led to fairly consistent results with only small to moderate changes in the derived emission rate, and how the choice of wind product had the largest influence on the derived emission, highlighting the importance of using winds from multiple sources. We also demonstrated the value of processing ESA and IUP-UB TROPOMI datasets in parallel, increasing the TROPOMI plume dataset by ~20% in this case. An in-depth analysis of the influence of wind variability around the time of overpass was conducted for both TROPOMI and GHGSat, with a small reduction in average TROPOMI emissions during flip vs. non-flip days, compared to little difference in GHGSat, highlighting the importance of a thorough review of meteorological effects for a given source.

More generally, this work shows the high-value potential for satellites to support local and regional emission reporting of more diffuse emission sources like landfills, allowing for an increasingly detailed dissection and interpretation of contributing sources from TROPOMI-scales through to point source imagers and aircraft measurements. More work should

https://doi.org/10.5194/egusphere-2026-3797
Preprint. Discussion started: 31 August 2026

be done on formally evaluating the accuracy of satellites specifically for diffuse sources, the "completeness" of the observation due to detection limits and sensitivity to diffuse enhancements, the degree to which "snap-shot" measurements can be representative of annual emissions, and the degree to which the observed variability in emission is real compared to observational. Satellite remote sensing of methane emissions would further benefit from expanding the range of controlled release experiments designed to imitate truly diffuse sources, as well as coordinated direct in-situ plume measurement of real landfill emissions to compare directly remotely-sensed emissions. The above are all active areas of research and development within the community.

Satellites have identified clear discrepancies between top-down measurement-based and bottom-up estimate-based emission rates for a variety of sectors, including waste. Traditional bottom-up approaches, whilst accepted by regulatory bodies, rely on emission factors and activity data that may not reflect actual operational conditions and therefore may not represent real-world emissions, with direct financial and regulatory implications for the emitting facilities. These discrepancies weaken the accuracy of the reporting that is crucial for the design of effective and targeted mitigation policy, and also propagate as an under-representation of emissions within the national inventories, climate models, and regulatory frameworks that rely on them. Satellite-based monitoring offers a transformative step towards closing this gap, providing routine, independent, and spatially resolved measurements which can help evaluate reported emissions and inform the design of effective mitigation.

One of the limitations identified by this work was the challenge of reconciling the differences in sensitivity and measurement technique between methods. This challenge could be overcome through dedicated intercomparison with coordinated and coincident in situ and remote measurements. Following the work presented here, we have developed a collaborative relationship with Madrid City Council, the owners of the Las Dehesas Landfill. Thanks to this relationship, we co-designed and undertook a dedicated, multiphase Leak Detection and Repair campaign (LDAR) in 2025 using coordinated aircraft, satellite, and tracer gas dispersion measurements, combined with more traditional on-site OGI surveys, to identify precise leak locations, quantify whole site emissions, support remedial works, and then evaluate the effectiveness of remediations. The LDAR campaign should demonstrate the potential for using multiple complementary techniques for effective methane monitoring and informed mitigation.

Data availability

The ESA operational Sentinel-5P TROPOMI XCH_4 and Sentinel-2 data are available at the Copernicus Data Hub via https://dataspace.copernicus.eu. The IUP-UB Sentinel-5P TROPOMI/WFMD XCH4 product is available at https://www.iup.uni-bremen.de/carbon_ghg/products/tropomi_wfmd/. ERA5 Reanalysis data is available at https://cds.climate.copernicus.eu/. GEOS-FP data is available at https://portal.nccs.nasa.gov/. Wind measurements from local Madrid air quality stations are available at https://datos.comunidad.madrid/. CAMS and EDGAR emission inventories are available at https://eccad.aeris-data.fr/ and https://edgar.jrc.ec.europa.eu/ respectfully. PRTR-España data is available at

https://doi.org/10.5194/egusphere-2026-3797
Preprint. Discussion started: 31 August 2026

https://en.prtr-es.miteco.gob.es/, for Pinto (Facility 1458) and Las Dehesas (Facility 3164). GHGSat data used in this analysis can be made available upon request.

Acknowledgements

This study was carried out as part of the MEDUSA project (Methane Emissions Detection Using Satellites Assessment) funded by the European Space Agency (ESA Contract no. 4000143908/24/I-LR). This work evolved from an EDAP+ validation study on GHGSat (EDAP+.REP.026), which includes the 2022 GHGSat airborne data funded by ESA. We thank the team that realized the TROPOMI instrument, consisting of the partnership between Airbus Defence and Space Netherlands, KNMI, SRON, and TNO, commissioned by NSO and ESA. We thank those responsible for the development of the TROPOMI XCH_4 retrieval products, namely the operational ESA product by SRON and the WFM-DOAS IUP-UB product by the University of Bremen. The Sentinel-5 Precursor and Sentinel-2 are part of the EU Copernicus programme, and Copernicus (modified) Sentinel-5P data (2019–2024) and Sentinel-2 data (2020–2024) have been used. We thank GHGSat for the production of emission data from their GHGSat satellite constellation and aircraft instrument, and for support during data analysis. Access to the GHGSat catalogue was provided through the Methane Monitoring Data Supply for the UK, facilitated by the Satellite Applications Catapult, funded by the UK Space Agency (UKSA). D.A.P. and H.S. acknowledge the use of the University of Leicester High Performance Computing facility ALICE to conduct data processing and analysis.

Author contributions

H.S., J.D.M., and I.A. designed the study. B.J.S. and M.D. produced the ESA_{ML} emission dataset. O.S. provided the IUP-UB WFMD CH_4 concentration dataset. D.A.P. produced the ESA_{SB} and IUP_{SB} emission datasets and performed the analysis and interpretation of all datasets. D.A.P. wrote the manuscript with input from all co-authors.

Competing interests

The authors declare that they have no competing interests.

Financial support

This study was carried out as part of the MEDUSA project (Methane Emissions Detection Using Satellites Assessment) funded by the European Space Agency's Climate Change Initiative. University of Bremen contributions received funding from the European Space Agency (ESA) via the projects GHG-CCI+ and SMART-CH4 (ESA contract nos. 4000126450/19/I-NB and 4000142730/23/I-NS) and from the Federal Ministry of Research, Technology and Space (BMFTR) within its project ITMS via grant no. 01 LK2103A. The TROPOMI/WFMD retrievals were performed on HPC facilities of the IUP, University of Bremen, funded under DFG/FUGG grant nos. INST 144/379-1 and INST 144/493-1.

References

El Abbadi, S. H., Chen, Z., Burdeau, P. M., Rutherford, J. S., Chen, Y., Zhang, Z., Sherwin, E. D., and Brandt, A. R.: Technological Maturity of Aircraft-Based Methane Sensing for Greenhouse Gas Mitigation, Environ. Sci. Technol., 58, 9591–9600, https://doi.org/10.1021/ACS.EST.4C02439/ASSET/IMAGES/LARGE/ES4C02439_0004.JPEG, 2024.

Agency, E.: Investigating variability in landfill methane emissions using air quality monitoring data - report, https://www.gov.uk/government/publications/investigating-variability-in-landfill-methane-emissions-using-air-quality-monitoring-data, 2024.

Aghdam, E. F., Scheutz, C., and Kjeldsen, P.: Impact of meteorological parameters on extracted landfill gas composition and flow, Waste Management, 87, 905–914, https://doi.org/10.1016/j.wasman.2018.01.045, 2019.

Allen, G., Hollingsworth, P., Kabbabe, K., Pitt, J. R., Mead, M. I., Illingworth, S., Roberts, G., Bourn, M., Shallcross, D. E., and Percival, C. J.: The development and trial of an unmanned aerial system for the measurement of methane flux from landfill and greenhouse gas emission hotspots, Waste Management, 87, 883–892, https://doi.org/10.1016/j.wasman.2017.12.024, 2019.

Publications - IPCC-TFI: https://www.ipcc-nggip.iges.or.jp/public/2006gl/vol5.html, last access: 12 March 2026.

Apituley, A., Pedergnana, M., Sneep, M., Veefkind, J. P., Loyola, D., and Hasekamp, O.: Sentinel-5 precursor/TROPOMI Level 2 Product User Manual Methane, 2017.

Barry, R.: Mountain weather and climate, https://doi.org/10.4324/9780203416020/MOUNTAIN-WEATHER-CLIMATE-ROGER-BARRY, 2013.

Bhardwaj, P., Kumar, R., Mitchell, D. A., Randles, C. A., Downey, N., Blewitt, D., and Kosovic, B.: Evaluating the detectability of methane point sources from satellite observing systems using microscale modeling, Scientific Reports 2022 12:1, 12, 1–9, https://doi.org/10.1038/s41598-022-20567-z, 2022.

Bogner, J. E., Spokas, K. A., and Chanton, J. P.: Seasonal Greenhouse Gas Emissions (Methane, Carbon Dioxide, Nitrous Oxide) from Engineered Landfills: Daily, Intermediate, and Final California Cover Soils, J. Environ. Qual., 40, 1010–1020, https://doi.org/10.2134/jeq2010.0407, 2011.

Chanton, J. P., Powelson, D. K., and Green, R. B.: Methane Oxidation in Landfill Cover Soils, is a 10% Default Value Reasonable?, J. Environ. Qual., 38, 654–663, https://doi.org/10.2134/jeq2008.0221, 2009.

Crippa, M., Guizzardi, D., Pisoni, E., Solazzo, E., Guion, A., Muntean, M., Florczyk, A., Schiavina, M., Melchiorri, M., & Hutfilter, A. F. (2021). Global anthropogenic emissions in urban areas: patterns, trends, and challenges. *Environmental Research Letters*, *16*(7), 074033. https://doi.org/10.1088/1748-9326/AC00E2

Cusworth, D. H., Jacob, D. J., Varon, D. J., Chan Miller, C., Liu, X., Chance, K., Thorpe, A. K., Duren, R. M., Miller, C. E., Thompson, D. R., Frankenberg, C., Guanter, L., and Randles, C. A.: Potential of next-generation imaging spectrometers to detect and quantify methane point sources from space, Atmos. Meas. Tech., 12, 5655–5668, https://doi.org/10.5194/AMT-12-5655-2019, 2019.

Cusworth, D. H., Duren, R. M., Ayasse, A. K., Jiorle, R., Howell, K., Aubrey, A., Green, R. O., Eastwood, M. L., Chapman, J. W., Thorpe, A. K., Heckler, J., Asner, G. P., Smith, M. L., Thoma, E., Krause, M. J., Heins, D., and Thorneloe, S.: Quantifying methane emissions from United States landfills, Science, 383, 1499–1504, https://doi.org/10.1126/SCIENCE.ADI7735, 2024.

Czepiel, P. M., Shorter, J. H., Mosher, B., Allwine, E., McManus, J. B., Harriss, R. C., Kolb, C. E., and Lamb, B. K.: The influence of atmospheric pressure on landfill methane emissions, Waste Management, 23, 593–598, https://doi.org/10.1016/S0956-053X(03)00103-X, 2003.

Defratyka, S. M., Paris, J. D., Yver-Kwok, C., Fernandez, J. M., Korben, P., and Bousquet, P.: Mapping Urban Methane Sources in Paris, France, Environ. Sci. Technol., 55, 8583–8591, https://doi.org/10.1021/acs.est.1c00859, 2021.

Dogniaux, M., Maasakkers, J. D., Girard, M., Jervis, D., McKeever, J., Schuit, B. J., Sharma, S., Lopez-Noreña, A., Varon, D. J., and Aben, I.: Global satellite survey reveals uncertainty in landfill methane emissions, Nature 2025 647:8089, 647, 397–402, https://doi.org/10.1038/s41586-025-09683-8, 2025.

Duan, Z., Kjeldsen, P., and Scheutz, C.: Efficiency of gas collection systems at Danish landfills and implications for regulations, Waste Management, 139, 269–278, https://doi.org/10.1016/J.WASMAN.2021.12.023, 2022.

Dubey, L., Cooper, J., and Hawkes, A.: Minimum detection limits of the TROPOMI satellite sensor across North America and their implications for measuring oil and gas methane emissions, Science of the Total Environment, 872, https://doi.org/10.1016/J.SCITOTENV.2023.162222, 2023.

Eldering, A.: Methane Plume Detection and Quantification Intercomparison Analysis Based on EMIT Measurements, https://doi.org/https://datafoundation.org/news/reports/812/812-Methane-Plume-Detection-and-Quantification-Intercomparison-Analysis-Based-on-EMIT-Measurements-, 2026.

Emran, B. J., Tannant, D. D., and Najjaran, H.: Low-Altitude Aerial Methane Concentration Mapping, Remote Sensing 2017, Vol. 9, Page 823, 9, 823, https://doi.org/10.3390/rs9080823, 2017.

FluxLab: Simulation Facility for Landfill Emission Experiments (SIMFLEX). https://fluxlab.ca/simflex/, last access: 5 March 2026.

Frankenberg, C., Thorpe, A. K., Thompson, D. R., Hulley, G., Kort, E. A., Vance, N., Borchardt, J., Krings, T., Gerilowski, K., Sweeney, C., Conley, S., Bue, B. D., Aubrey, A. D., Hook, S., and Green, R. O.: Airborne methane remote measurements reveal heavytail flux distribution in Four Corners region, Proc. Natl. Acad. Sci. U. S. A., 113, 9734–9739, https://doi.org/10.1073/PNAS.1605617113, 2016.

Ganesan, A. L., Schwietzke, S., Poulter, B., Arnold, T., Lan, X., Rigby, M., Vogel, F. R., van der Werf, G. R., Janssens-Maenhout, G., Boesch, H., Pandey, S., Manning, A. J., Jackson, R. B., Nisbet, E. G., and Manning, M. R.: Advancing Scientific Understanding of the Global Methane Budget in Support of the Paris Agreement, Global Biogeochem. Cycles, 33, 1475–1512, https://doi.org/10.1029/2018GB006065, 2019.

Gao, M., Xing, Z., Vollrath, C., Hugenholtz, C. H., and Barchyn, T. E.: Global observational coverage of onshore oil and gas methane sources with TROPOMI, Scientific Reports 2023 13:1, 13, 1–11, https://doi.org/10.1038/s41598-023-41914-8, 2023.

Giordano, C. R., Van Brunt, M. E., Halevi, S. J., Castaldi, M. J., Orlovits, Z., and Illes, Z.: Landfill gas collection efficiency: Categorization of data from existing in-situ measurements, Waste Management, 175, 83–91, https://doi.org/10.1016/j.wasman.2023.12.042, 2024.

Hersbach, H., Bell, B., Berrisford, P., Hirahara, S., Horányi, A., Muñoz-Sabater, J., Nicolas, J., Peubey, C., Radu, R., Schepers, D., Simmons, A., Soci, C., Abdalla, S., Abellan, X., Balsamo, G., Bechtold, P., Biavati, G., Bidlot, J., Bonavita, M., De Chiara, G., Dahlgren, P., Dee, D., Diamantakis, M., Dragani, R., Flemming, J., Forbes, R., Fuentes, M., Geer, A., Haimberger, L., Healy, S., Hogan, R. J., Hólm, E., Janisková, M., Keeley, S., Laloyaux, P., Lopez, P., Lupu, C., Radnoti, G., de Rosnay, P., Rozum, I., Vamborg, F., Villaume, S., and Thépaut, J. N.: The ERA5 global reanalysis, Quarterly Journal of the Royal Meteorological Society, 146, 1999–2049, https://doi.org/10.1002/QJ.3803, 2020.

Hoinka, K. P. and De Castro, M.: The Iberian Peninsula thermal low, Quarterly Journal of the Royal Meteorological Society, 129, 1491–1511, https://doi.org/10.1256/QJ.01.189;WEBSITE:WEBSITE:RMETS, 2003.

Iftakhar Hossain, R., Buntov, P., Dudak, Y., Martino, R., Fougere, C., Naseridoust, S., Bourlon, E., Lavoie, M., khaleghi, afshan, Hall, C., and Risk, D.: A controlled release experiment for investigating methane measurement performance at landfills, https://doi.org/10.31223/X5F72M, 2025.

Jacob, D. J., Turner, A. J., Maasakkers, J. D., Sheng, J., Sun, K., Liu, X., Chance, K., Aben, I., McKeever, J., and Frankenberg, C.: Satellite observations of atmospheric methane and their value for quantifying methane emissions, Atmos. Chem. Phys., 16, 14371–14396, https://doi.org/10.5194/ACP-16-14371-2016, 2016.

Jervis, D., McKeever, J., Durak, B. O. A., Sloan, J. J., Gains, D., Varon, D. J., Ramier, A., Strupler, M., and Tarrant, E.: The GHGSat-D imaging spectrometer, Atmos. Meas. Tech., 14, 2127–2140, https://doi.org/10.5194/AMT-14-2127-2021, 2021.

Jongaramrungruang, S., Frankenberg, C., Matheou, G., Thorpe, A. K., Thompson, D. R., Kuai, L., and Duren, R. M.: Towards accurate methane point-source quantification from high-resolution 2-D plume imagery, Atmos. Meas. Tech., 12, 6667–6681, https://doi.org/10.5194/amt-12-6667-2019, 2019.

Kashyap, R. K., Chugh, P., and Nandakumar, T.: Opportunities & Challenges in Capturing Landfill Gas from an Active and Un-scientifically Managed Land Fill Site – A Case Study, Procedia Environ. Sci., 35, 348–367, https://doi.org/10.1016/J.PROENV.2016.07.015, 2016.

Kissas, K., Ibrom, A., Kjeldsen, P., and Scheutz, C.: Methane emission dynamics from a Danish landfill: The effect of changes in barometric pressure, Waste Management, 138, 234–242, https://doi.org/10.1016/J.WASMAN.2021.11.043, 2022.

Krautwurst, S., Fruck, C., Wolff, S., Borchardt, J., Huhs, O., Gerilowski, K., Gałkowski, M., Kiemle, C., Quatrevalet, M., Wirth, M., Mallaun, C., Burrows, J. P., Gerbig, C., Fix, A., Bösch, H., and Bovensmann, H.: Identification and quantification of CH4 emissions from Madrid landfills using airborne imaging spectrometry and greenhouse gas lidar, Atmos. Chem. Phys., 25, 14669–14702, https://doi.org/10.5194/acp-25-14669-2025, 2025.

https://doi.org/10.5194/egusphere-2026-3797
Preprint. Discussion started: 31 August 2026

Krings, T., Gerilowski, K., Buchwitz, M., Reuter, M., Tretner, A., Erzinger, J., Heinze, D., Pflüger, U., Burrows, J. P., and Bovensmann, H.: MAMAP - A new spectrometer system for column-averaged methane and carbon dioxide observations from aircraft: Retrieval algorithm and first inversions for point source emission rates, Atmos. Meas. Tech., 4, 1735–1758, https://doi.org/10.5194/AMT-4-1735-2011, 2011.

Kumar, P., Caldow, C., Broquet, G., Shah, A., Laurent, O., Yver-Kwok, C., Ars, S., Defratyka, S., Gichuki, S. W., Lienhardt, L., Lozano, M., Paris, J. D., Vogel, F., Bouchet, C., Allegrini, E., Kelly, R., Juery, C., and Ciais, P.: Detection and long-term quantification of methane emissions from an active landfill, Atmos. Meas. Tech., 17, 1229–1250, https://doi.org/10.5194/AMT-17-1229-2024, 2024.

Kurniawan, T. A., Liang, X., Singh, D., Othman, M. H. D., Goh, H. H., Gikas, P., Kern, A. O., Kusworo, T. D., and Shoqeir, J. A.: Harnessing landfill gas (LFG) for electricity: A strategy to mitigate greenhouse gas (GHG) emissions in Jakarta (Indonesia), J. Environ. Manage., 301, 113882, https://doi.org/10.1016/J.JENVMAN.2021.113882, 2022.

Lorente, A., Borsdorff, T., Butz, A., Hasekamp, O., Aan De Brugh, J., Schneider, A., Wu, L., Hase, F., Kivi, R., Wunch, D., Pollard, D. F., Shiomi, K., Deutscher, N. M., Velazco, V. A., Roehl, C. M., Wennberg, P. O., Warneke, T., and Landgraf, J.: Methane retrieved from TROPOMI: Improvement of the data product and validation of the first 2 years of measurements, Atmos. Meas. Tech., 14, 665–684, https://doi.org/10.5194/AMT-14-665-2021, 2021.

Lorente, A., Borsdorff, T., Martinez-Velarte, M. C., and Landgraf, J.: Accounting for surface reflectance spectral features in TROPOMI methane retrievals, Atmos. Meas. Tech., 16, 1597–1608, https://doi.org/10.5194/AMT-16-1597-2023, 2023.

Maasakkers, J. D., Varon, D. J., Elfarsdóttir, A., McKeever, J., Jervis, D., Mahapatra, G., Pandey, S., Lorente, A., Borsdorff, T., Foorthuis, L. R., Schuit, B. J., Tol, P., Van Kempen, T. A., Van Hees, R., and Aben, I.: Using satellites to uncover large methane emissions from landfills, Sci. Adv., 8, https://doi.org/10.1126/SCIADV.ABN9683, 2022.

Meyer-Dombard, D. R., Bogner, J. E., and Malas, J.: A Review of Landfill Microbiology and Ecology: A Call for Modernization With 'Next Generation' Technology, Front. Microbiol., 11, 537641, https://doi.org/10.3389/FMICB.2020.01127/BIBTEX, 2020.

MITECO Memoria anual de generación y gestión de residuos: https://www.miteco.gob.es/es/calidad-y-evaluacion-ambiental/publicaciones/memoria-anual-generacion-gestion-residuos.html#residuos-de-competencia-municipal, last access: 20 April 2026.

Molod, A., Takacs, L., Suarez, M., Bacmeister, J., Song, I.-S., Eichmann, A., and Suarez, M. J.: The GEOS-5 Atmospheric General Circulation Model: Mean Climate and Development from MERRA to Fortuna, http://www.sti.nasa.gov, 2012.

Mønster, J., Kjeldsen, P., and Scheutz, C.: Methodologies for measuring fugitive methane emissions from landfills – A review, Waste Management, 87, 835–859, https://doi.org/10.1016/j.wasman.2018.12.047, 2019.

Nesser, H., Jacob, D. J., Maasakkers, J. D., Lorente, A., Chen, Z., Lu, X., Shen, L., Qu, Z., Sulprizio, M. P., Winter, M., Ma, S., Bloom, A. A., Worden, J. R., Stavins, R. N., and Randles, C. A.: High-resolution US methane emissions inferred

https://doi.org/10.5194/egusphere-2026-3797
Preprint. Discussion started: 31 August 2026

from an inversion of 2019 TROPOMI satellite data: contributions from individual states, urban areas, and landfills, Atmos. Chem. Phys., 24, 5069–5091, https://doi.org/10.5194/ACP-24-5069-2024, 2024.

Nisbet-Jones, P. B. R., Fernandez, J. M., Fisher, R. E., France, J. L., Lowry, D., Waltham, D. A., Woolley Maisch, C. A., and Nisbet, E. G.: Is the destruction or removal of atmospheric methane a worthwhile option?, Philosophical Transactions of the Royal Society A, 380, https://doi.org/10.1098/RSTA.2021.0108, 2022.

Omidi, A., Bourlon, E., Khaleghi, A., Perrine, G., Tarakki, N., Martino, R., Stuart, J., and Risk, D.: Active face emissions: An opportunity for reducing methane emissions in global waste management, Elem Sci Anth, 13, https://doi.org/10.1525/elementa.2025.00042, 2025.

Poulsen Tjalfe G., G., Christophersen, M., Moldrup, P., and Kjeldsen, P.: Relating landfill gas emissions to atmospheric pressure using numerical modelling and state-space analysis, Waste Management & Research, 21, 356–366, https://doi.org/10.1177/0734242X0302100408, 2003.

Rachor, I. M., Gebert, J., Gröngröft, A., and Pfeiffer, E. M.: Variability of methane emissions from an old landfill over different time-scales, Eur. J. Soil Sci., 64, 16–26, https://doi.org/10.1111/EJSS.12004;WGROUP:STRING:PUBLICATION, 2013.

Sadavarte, P., Pandey, S., Maasakkers, J. D., Lorente, A., Borsdorff, T., Denier Van Der Gon, H., Houweling, S., and Aben, I.: Methane emissions from superemitting coal mines in Australia quantified using TROPOMI satellite observations, ACS Publications, 55, 16573–16580, https://doi.org/10.1021/acs.est.1c03976, 2021.

Santolaria, E.: Local and regional characterisation of the diurnal mountain wind systems in the Guadarrama mountain range (Spain), https://www.academia.edu/89059255/Local_and_regional_characterisation_of_the_diurnal_mountain_wind_systems_in_ the_Guadarrama_mountain_range_Spain, 1 January 2017.

Saunois, M., Martinez, A., Poulter, B., Zhang, Z., Raymond, P. A., Regnier, P., Canadell, J. G., Jackson, R. B., Patra, P. K., Bousquet, P., Ciais, P., Dlugokencky, E. J., Lan, X., Allen, G. H., Bastviken, D., Beerling, D. J., Belikov, D. A., Blake, D. R., Castaldi, S., Crippa, M., Deemer, B. R., Dennison, F., Etiope, G., Gedney, N., Höglund-Isaksson, L., Holgerson, M. A., Hopcroft, P. O., Hugelius, G., Ito, A., Jain, A. K., Janardanan, R., Johnson, M. S., Kleinen, T., Krummel, P. B., Lauerwald, R., Li, T., Liu, X., Mcdonald, K. C., Melton, J. R., Mühle, J., Müller, J., Murguia-Flores, F., Niwa, Y., Noce, S., Pan, S., Parker, R. J., Peng, C., Ramonet, M., Riley, W. J., Rocher-Ros, G., Rosentreter, J. A., Sasakawa, M., Segers, A., Smith, S. J., Stanley, E. H., Thanwerdas, J., Tian, H., Tsuruta, A., Tubiello, F. N., Weber, T. S., Van Der Werf, G. R., Worthy, D. E. J., Xi, Y., Yoshida, Y., Zhang, W., Zheng, B., Zhu, Q., Zhu, Q., and Zhuang, Q.: Global Methane Budget 2000-2020, Earth Syst. Sci. Data, 17, 1873–1958, https://doi.org/10.5194/ESSD-17-1873-2025, 2025.

Scarpelli, T. R., Cusworth, D. H., Duren, R. M., Kim, J., Heckler, J., Asner, G. P., Thoma, E., Krause, M. J., Heins, D., and Thorneloe, S.: Investigating Major Sources of Methane Emissions at US Landfills, Environ. Sci. Technol., 58, 21545–21556, https://doi.org/10.1021/acs.est.4c07572, 2024.

Scheutz, C., Samuelsson, J., Fredenslund, A. M., and Kjeldsen, P.: Quantification of multiple methane emission sources at landfills using a double tracer technique, Waste Management, 31, 1009–1017, https://doi.org/10.1016/j.wasman.2011.01.015, 2011.

Schneising, O., Buchwitz, M., Reuter, M., Vanselow, S., Bovensmann, H., and P. Burrows, J.: Remote sensing of methane leakage from natural gas and petroleum systems revisited, Atmos. Chem. Phys., 20, 9169–9182, https://doi.org/10.5194/ACP-20-9169-2020, 2020.

Schneising, O., Bovensmann, H., Buchwitz, M., Buschmann, M., Deutscher, N. M., Griffith, D. W. T., Hachmeister, J., Hase, F., Iraci, L. T., Kivi, R., Morino, I., Ohyama, H., Petri, C., Reuter, M., Robinson, J., Roehl, C., Sha, M. K., Shiomi, K., Strong, K., Sussmann, R., Té, Y., Velazco, V. A., Vrekoussis, M., Wang, W., Warneke, T., Weidmann, D., Wunch, D., Zhou, M., and Bösch, H.: TROPOMI/WFMD v2.0: Improved retrievals of XCH4 and XCO with XGBoost-based quality filtering, Atmos. Meas. Tech., 19, 2407–2435, https://doi.org/10.5194/amt-19-2407-2026, 2026.

Schuit, B. J., Maasakkers, J. D., Bijl, P., Mahapatra, G., Van Den Berg, A. W., Pandey, S., Lorente, A., Borsdorff, T., Houweling, S., Varon, D. J., McKeever, J., Jervis, D., Girard, M., Irakulis-Loitxate, I., Gorroño, J., Guanter, L., Cusworth, D. H., and Aben, I.: Automated detection and monitoring of methane super-emitters using satellite data, Atmos. Chem. Phys., 23, 9071–9098, https://doi.org/10.5194/ACP-23-9071-2023, 2023.Shen, L., Jacob, D. J., Gautam, R., Omara, M., Scarpelli, T. R., Lorente, A., Zavala-Araiza, D., Lu, X., Chen, Z., and Lin, J.: National quantifications of methane emissions from fuel exploitation using high resolution inversions of satellite observations, Nature Communications 2023 14:1, 14, 1–9, https://doi.org/10.1038/s41467-023-40671-6, 2023.

Sherwin, E. D., Rutherford, J. S., Chen, Y., Aminfard, S., Kort, E. A., Jackson, R. B., and Brandt, A. R.: Single-blind validation of space-based point-source detection and quantification of onshore methane emissions, Sci. Rep., 13, https://doi.org/10.1038/S41598-023-30761-2, 2023.

Sherwin, E. D., El Abbadi, S. H., Burdeau, P. M., Zhang, Z., Chen, Z., Rutherford, J. S., Chen, Y., and Brandt, A. R.: Single-blind test of nine methane-sensing satellite systems from three continents, Atmos. Meas. Tech., 17, 765–782, https://doi.org/10.5194/AMT-17-765-2024, 2024.

Sirimangkhala, K., Pimpunchat, B., Amornsamankul, S., and Triamp, W.: Modelling Greenhouse Gas Generation for Landfill, International journal of simulation: systems, science & technology, https://doi.org/10.5013/ijssst.a.19.04.16, 2018.

Skeie, R. B., Hodnebrog, Ø., and Myhre, G.: Trends in atmospheric methane concentrations since 1990 were driven and modified by anthropogenic emissions, Commun. Earth Environ., 4, 1–14, https://doi.org/10.1038/S43247-023-00969-1;SUBJMETA=106,35,47,704,824;KWRD=ATMOSPHERIC+CHEMISTRY,BIOGEOCHEMISTRY, 2023.

Srikanth, A., Stokes, S., Yang, S., and Ravikumar, A.: Understanding Trends in Methane Emissions from Landfills through Repeat Aerial Surveys, https://doi.org/10.26434/chemrxiv-2025-77s45, 2025.

Townsend-Small, A., Tyler, S. C., Pataki, D. E., Xu, X., and Christensen, L. E.: Isotopic measurements of atmospheric methane in Los Angeles, California, USA: Influence of “fugitive” fossil fuel emissions, Journal of Geophysical Research Atmospheres, 117, https://doi.org/10.1029/2011JD016826, 2012.

https://doi.org/10.5194/egusphere-2026-3797
Preprint. Discussion started: 31 August 2026

Tu, Q., Hase, F., Schneider, M., Garciá, O., Blumenstock, T., Borsdorff, T., Frey, M., Khosrawi, F., Lorente, A., Alberti, C., Bustos, J. J., Butz, A., Carreño, V., Cuevas, E., Curcoll, R., Diekmann, C. J., Dubravica, D., Ertl, B., Estruch, C., León-Luis, S. F., Marrero, C., Morgui, J. A., Ramos, R., Scharun, C., Schneider, C., Sepúlveda, E., Toledano, C., and Torres, C.: Quantification of CH4 emissions from waste disposal sites near the city of Madrid using ground- and space-based observations of COCCON, TROPOMI and IASI, Atmos. Chem. Phys., 22, 295–317, https://doi.org/10.5194/ACP-22-295-2022, 2022a.

Tu, Q., Schneider, M., Hase, F., Khosrawi, F., Ertl, B., Necki, J., Dubravica, D., Diekmann, C. J., Blumenstock, T., and Fang, D.: Quantifying CH4 emissions in hard coal mines from TROPOMI and IASI observations using the wind-assigned anomaly method, Atmos. Chem. Phys., 22, 9747–9765, https://doi.org/10.5194/acp-22-9747-2022, 2022b.

Valdemingomez Technology Park.: Memoria de actividades annual public report 2023. https://www.madrid.es/portales/munimadrid/es/Inicio/Medio-ambiente/Parque-Tecnologico-Valdemingomez/Publicaciones/Memorias-de-gestion-de-la-DGPTV/?vgnextchannel=878d0b7d262e8810VgnVCM1000001d4a900aRCRD Last accessed: 20th April 2026.

Varon, D. J., Jacob, D. J., McKeever, J., Jervis, D., Durak, B. O. A., Xia, Y., and Huang, Y.: Quantifying methane point sources from fine-scale satellite observations of atmospheric methane plumes, Atmos. Meas. Tech., 11, 5673–5686, https://doi.org/10.5194/AMT-11-5673-2018, 2018.

Varon, D. J., McKeever, J., Jervis, D., Maasakkers, J. D., Pandey, S., Houweling, S., Aben, I., Scarpelli, T., and Jacob, D. J.: Satellite Discovery of Anomalously Large Methane Point Sources From Oil/Gas Production, Geophys. Res. Lett., 46, 13507–13516, https://doi.org/10.1029/2019GL083798, 2019.

Veefkind, J. P., Serrano-Calvo, R., de Gouw, J., Dix, B., Schneising, O., Buchwitz, M., Barré, J., van der A, R. J., Liu, M., and Levelt, P. F.: Widespread Frequent Methane Emissions From the Oil and Gas Industry in the Permian Basin, Journal of Geophysical Research: Atmospheres, 128, e2022JD037479, https://doi.org/10.1029/2022JD037479, 2023.

Wang, Y., Fang, M., Lou, Z., He, H., Guo, Y., Pi, X., Wang, Y., Yin, K., and Fei, X.: Methane emissions from landfills differentially underestimated worldwide, Nat. Sustain., 7, 496–507, https://doi.org/10.1038/S41893-024-01307-9;SUBJMETA=166,172,4081,639,704,986;KWRD=CIVIL+ENGINEERING,ENVIRONMENTAL+IMPACT, 2024.

Whiteman, C.: Mountain meteorology: fundamentals and applications, 2000.

Whiteman, C. D.: Observations of Thermally Developed Wind Systems in Mountainous Terrain, Atmospheric Processes over Complex Terrain, 5–42, https://doi.org/10.1007/978-1-935704-25-6_2, 1990.

Yang, Z., Li, J., Liu, W., Yang, J., Sun, H., Shi, L., Yin, D., and Qin, K.: An Intercomparison of Underground Coal Mine Methane Emission Estimation in Shanxi, China: S5P/TROPOMI vs. GF-5B/AHSI, Remote Sensing 2026, Vol. 18, Page 603, 18, 603, https://doi.org/10.3390/rs18040603, 2026.

Yu, B., Zhu, B., Miao, S., Kang, H., He, X., Liu, H., Liang, Z., and Chen, F.: Observational Signal of the Interaction Between Mountain–Plain Wind and Urban Breeze Under Weak Synoptic Systems, Journal of Geophysical Research: Atmospheres, 126, e2020JD032809, https://doi.org/10.1029/2020JD032809, 2021.

https://doi.org/10.5194/egusphere-2026-3797
Preprint. Discussion started: 31 August 2026

Zardi, D. and Whiteman, C. D.: Diurnal Mountain Wind Systems, 35–119, https://doi.org/10.1007/978-94-007-4098-3_2, 2013.

Zhang, C. X., Zhang, Z. N., Wang, Y. X., and Mebra, O.: Methane distribution surrounding closed landfill sites in China, Environmental Technology (United Kingdom), 33, 2159–2166, https://doi.org/10.1080/09593330.2012.660654, 2012.

Zhang, X., Maasakkers, J. D., Roger, J., Guanter, L., Sharma, S., Lama, S., Tol, P., Varon, D. J., Cusworth, D. H., Howell, K., Thorpe, A. K., Brodrick, P. G., and Aben, I.: Global Identification of Solid Waste Methane Super Emitters Using Hyperspectral Satellites, Environ. Sci. Technol., 59, 18134–18145, https://doi.org/10.1021/acs.est.4c14196, 2025.

https://doi.org/10.5194/egusphere-2026-3797
Preprint. Discussion started: 31 August 2026

Appendix

A1 CH4 emission derivation

Emission rates in all cases (excluding aircraft) are derived using the Integrated Mass Enhancement (IME) approach, detailed for satellite applications in (Varon et al., 2018) and used extensively for methane studies (Bhardwaj et al., 2022; Cusworth et al., 2019; Frankenberg et al., 2016; Jongaramrungruang et al., 2019; Varon et al., 2019). The aircraft used the Cross-Sectional Flux (CSF) method. TROPOMI and GHGSat approaches were calculated using wind information from GEOS-FP 10 m, ERA5 10 m, ERA5 PBL, in isolation and as ensemble. Additionally, emissions for GHGSat and aircraft were also calculated using local wind information from nearby air quality monitoring stations (Rivas-Vaciamadrid and Valmodero), and two local airports (Getafe air base and Madrid-Barajas), in an attempt to better describe local winds.

The TROPOMI methane plume detections provided for ESA_{ML} were obtained with an improved version of the automated plume detection framework presented in Schuit et al. (2023). This improved version uses the same Convolutional Neural Network (CNN) as in Schuit et al. (2023) to detect plume-like features in TROPOMI data, and employs a Random Forest Classifier (RFC) to filter artefacts instead of a Support Vector Classifier (SVC). All detections that pass these two steps are examined by two human operators in a quality control process, as for the TROPOMI plume detections provided each week by SRON to the Copernicus Atmosphere Monitoring Service (CAMS) (https://apps.atmosphere.copernicus.eu/methane-explorer/). Following Schuit et al. (2023), each plume is quantified using an ensemble approach which explores realistic value intervals for all the parameters relevant to the Integrated Mass Enhancement method (IME) to estimate uncertainty.

For the SB approach, for a given observation the wind direction from each wind product is used to create an upwind-downwind plume bounding box centred on the landfills. The upwind bbox characterises the local background, $\overline{CH4}$, bg, taken as the mean of the pixels within the upwind bounding box, chosen here as a region 10-30 km upwind from the source and 30

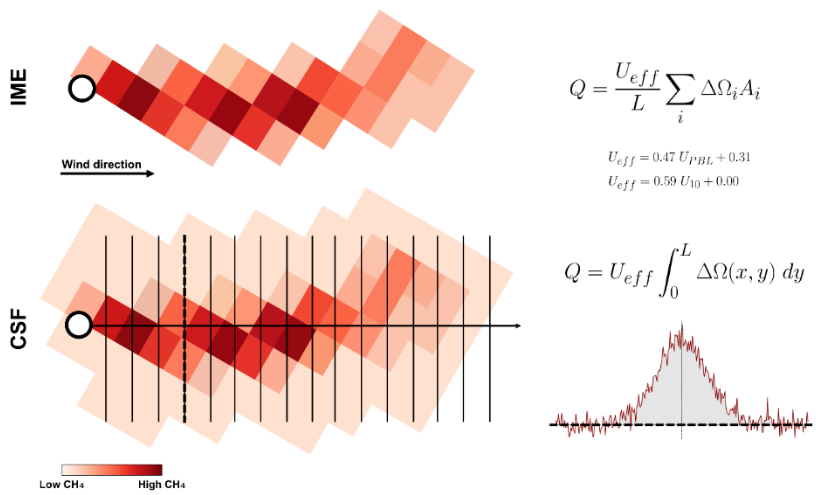

Figure A. 1: Illustration of IME and CSF emission derivation approaches

https://doi.org/10.5194/egusphere-2026-3797
Preprint. Discussion started: 31 August 2026

km wide. We chose to have this box begin upwind from the source location to account for the plume not starting at the centre point, as the plume will contain diffuse sources of CH4 from various sources, not just the landfills. This background is then subtracted from the XCH4 field to obtain a CH4 enhancement. The downwind bbox is chosen as a region from -20 to 75 km downwind from the source location, also 30 km wide. A threshold of 1.5σ is applied to the region of interest, to select sufficiently enhanced pixels above the background, which are then clustered together using a Density-Based Spatial Clustering of Applications with Noise (DBSCAN) approach. The pixel cluster closest to the source, with its closest pixel within 15 km of the source, is designated as the plume, and all other clusters are discarded. The mixing ratio enhancement in ppb is then converted to a mass enhancement using the molecular mass of CH4 and the vertical water vapour information in the TROPOMI data product to calculate the dry air column and convert into kg m^{-2}. We quantify an uncertainty for the emission source rate for each detected plume by taking the quadrature of selected sources of uncertainty which include: (1) the standard deviation of the local wind speed (σ_{ws}) and the average local wind speed including the ± 0.2° region around the sites (~ 35 x 35 km box, slightly larger than each model grid cell) and ± 1 hour preceding and following the overpass plus an additional base 2 m/s , (2) the standard deviation of the background XCH4 ($\sigma_{XCH_{4_{bg}}}$) and the average background, (3) the standard deviation of the plume enhancement CH4 ($\sigma_{CH_{4_{enh}}}$) and the average plume enhancement, and (4) the standard deviation of the XCH4 uncertainty ($\sigma_{CH_{4_{unc}}}$) from the IUP-UB XCH4 data.

A2 Sentinel-2 change detection

In order to relate methane plume origins observed by GHGSat, Sentinel-2 was used in combination with a change detection approach to identify both the area and timeframe of on-site activity, which represents the regions of the landfill being actively managed/constructed. First, cloud contaminated pixels were removed using the S2cloudless cloud detection approach. Scenes were cropped to the boundary of each landfill, and only 100% quality scenes were used, as any degree of missing pixels would invalidate the change detection approach. The change detection approach used here is similar to Dogniaux et al. (2025) in that an observation at time stamp, t, is compared to the closest observation before, t-1, and after, t+1. However, instead of using the Structural similarity (SSIM) index between observations, this approach utilises the Spectral Distance (SDist) between time stamps. The SDist approach compared the Euclidean Distance between all 13 bands (B1-B12), and between additional indices including Normalised Difference Vegetation Index (NDVI), Normalised Difference Water Index (NDWI), Brightness Index (BI) and Bare Soil Index (BSI). These additional indices increase sensitivity to changes specific to landfill activity, namely when bright dry soil is disturbed and replaced by darker fresh waste, and reduces sensitivity to shadows and topographical errors and specifically to variations due to the parallax effect. Landfill cells are raised mounds, and therefore present a parallax shift due to the changing viewing geometry of Sentinel-2 observations. Pixels with SDist > 3.5σ were identified as "changed", and coincident "changed" pixels between t-1 and t+1 compared to t were extracted as currently active pixels. These pixels were clustered using the Density-Based Spatial Clustering of Applications with Noise (DBSCAN)

https://doi.org/10.5194/egusphere-2026-3797
Preprint. Discussion started: 31 August 2026

clustering algorithm and stored along with their timestamp. This has been outlined in Figure A. 2. Clusters were then converted to convex hulls using the scipy ConvexHull tool, as in (Dogniaux et al., 2025).

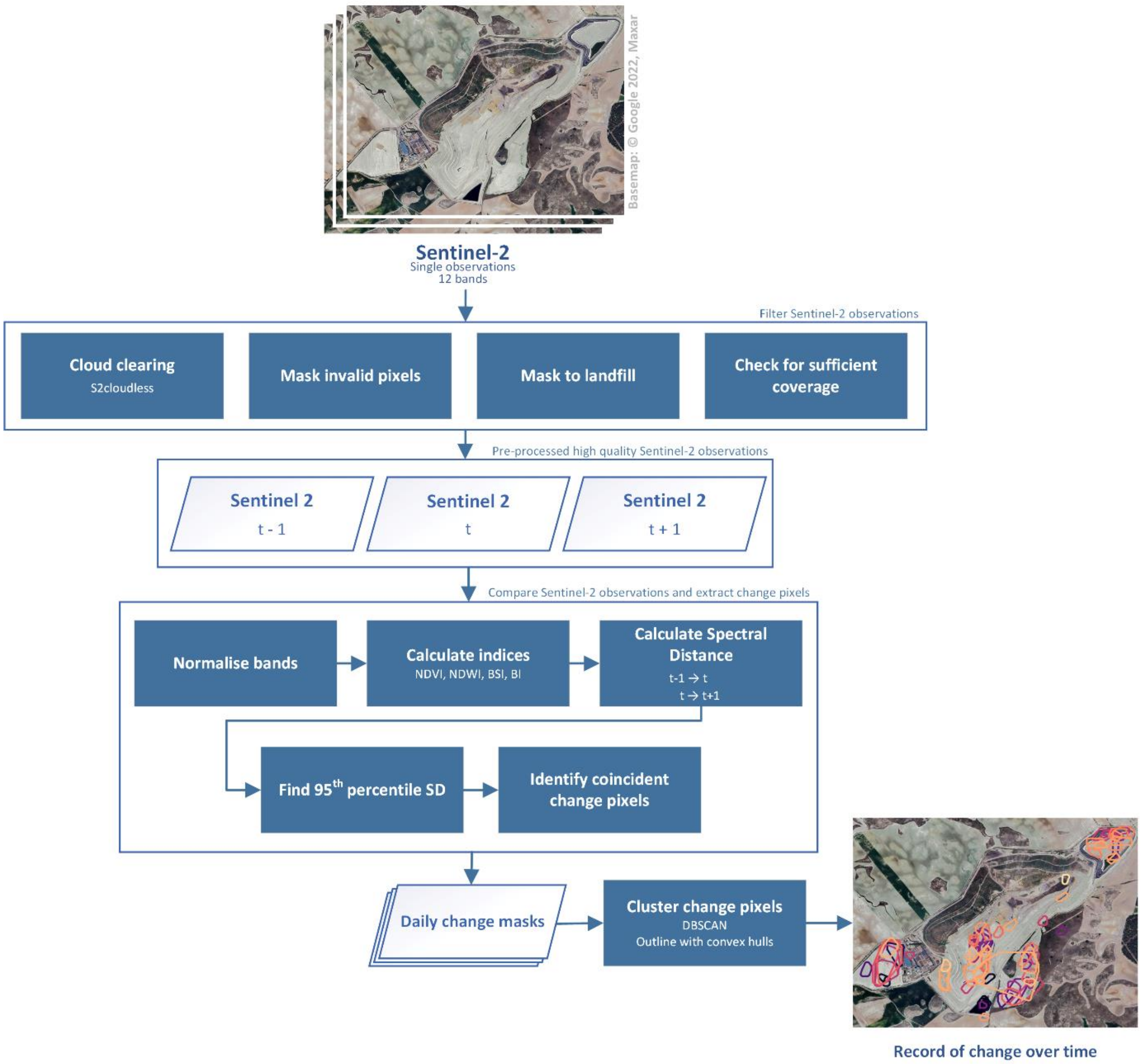

Figure A. 2: Outline of the S2 change detection approach, whereby L2-band Sentinel-2 observations of the landfill are ingested, quality checked, and clipped to the landfill ROI. Indices are calculated per-observation, from which the spectral distance is computed between each band and the preceeding/following observations. Regions of substantial spectral distance are identified as "changed", and stored as output.

https://doi.org/10.5194/egusphere-2026-3797
Preprint. Discussion started: 31 August 2026

A3 Wind flip

Madrid sits at the centre of the Iberian Peninsula on the expansive "Meseta Central" plateau (645 m above sea level). Madrid is located at the northeast end of the Tagus basin, with the Guadarrama and Somosierra mountain ranges, part of the Sistema Central Mountain range, to the north. These features influence the meteorology around Madrid and can drive strong and variable changes in meteorology over short time scales. The wind flip seen in Madrid is likely driven in part by diurnal mountain winds, which are then enhanced seasonally by the Iberian Thermal Low (ITL), due to Madrids proximity to the Guadarrama and Somosierra mountain ranges and position within the north eastern end of the Tagus basin (Hoinka and De Castro, 2003; Santolaria, 2017; Yu et al., 2021; Zardi and Whiteman, 2013). Diurnal Mountain winds have two phases, (i) valley breeze driven by anabatic flows (up-slope) during the daytime and (ii) mountain breeze driven by katabatic flows (down-slope) during the night (Whiteman, 2000, 1990). After sunrise, mountain slopes begin heating sooner than the valley floor, resulting in the warming of the airmass around the mountains. This thermal contrast leads to lower pressure at higher elevations. This pressure gradient draws up cooler air from the valley, driving an anabatic (up-slope) wind flow which forms a valley breeze (Barry, 2013). These winds grow in strength from the late morning until early afternoon, when solar heating reaches a peak. After this peak, heating reduces and radiative cooling begins, which reduces the thermal contrast between the mountains and the valley, where these upslope winds gradually weaken. Once the sun has set, the mountain slopes radiate heat quicker than the valley floor. The now cooler, denser mountain air sinks into the valley, driving the katabatic (down-slope) wind, forming a mountain breeze. Mountain breeze strength increases until sunrise, where the cycle repeats. The transition from valley to mountain breeze can take 2-4 hours from sunrise, and is dependent on the slope, altitude, cloud cover, and time of year.

In addition to this, the Iberian peninsula experiences synoptic-scale thermal lows during summer months (May – Sept). The dry, elevated land surface of central Spain heats rapidly, reducing air density and surface pressure, driving vertical motion through buoyant convection. This process deepens the boundary layer and leads to the formation of the ITL (Hoinka and De Castro, 2003). As the airmass rises, low-level convergence draws air from the southeast, where it is funnelled up through the tagus river basin, across Madrid, and out to the northeast.

As a result of these two complementary processes, Madrid often experiences nighttime northeasterly drainage winds which flow down the Tagus basin to the southwest and strong daytime southwesterly winds which flow northeast up the valley, with a transition between regimes around midday. This is seen clearly in Figure 9, as winds transition from one regime to another, leading to a reversal of wind direction. The Iberian peninsula is also subject to other synoptic-scale wind patterns due to it's position between the Atlantic and Medeterranean, which can often dominate over these processes. As such, whilst these processes may not always drive the local meteorology in Madrid, it is clear that there is a common 80-145° flip in wind direction around the time of the TROPOMI overpass.

https://doi.org/10.5194/egusphere-2026-3797
Preprint. Discussion started: 31 August 2026

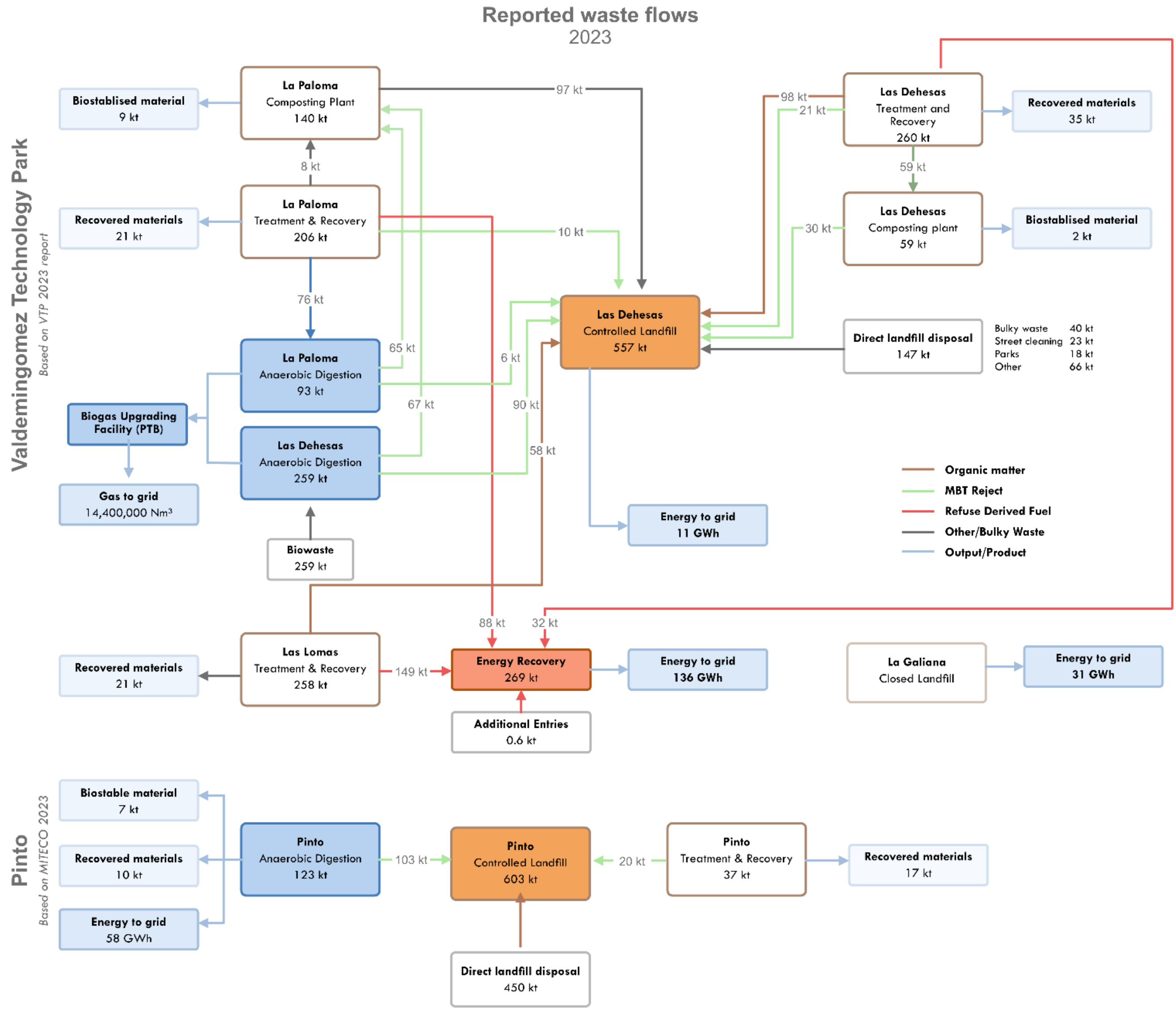

Figure A. 3: Diagram showing flows of waste for the VTP, Las Dehesas and Pinto landfill. Las Dehesas is based on VTP Memoria de actividades annual public reports (Valdemingomez, 2023). Pinto data is based on MITECO reported values, available at: https://www.miteco.gob.es/es/calidad-y-evaluacion-ambiental/publicaciones/memoria-anual-generacion-gestion-residuos.html. Data shown is for 2023. There are minor discrepancies between annual reported tonnage and the sum of tonnage through individual processes, as not all waste streams into the landfill are accounted for in the separate reporting schemes.

https://doi.org/10.5194/egusphere-2026-3797
Preprint. Discussion started: 31 August 2026

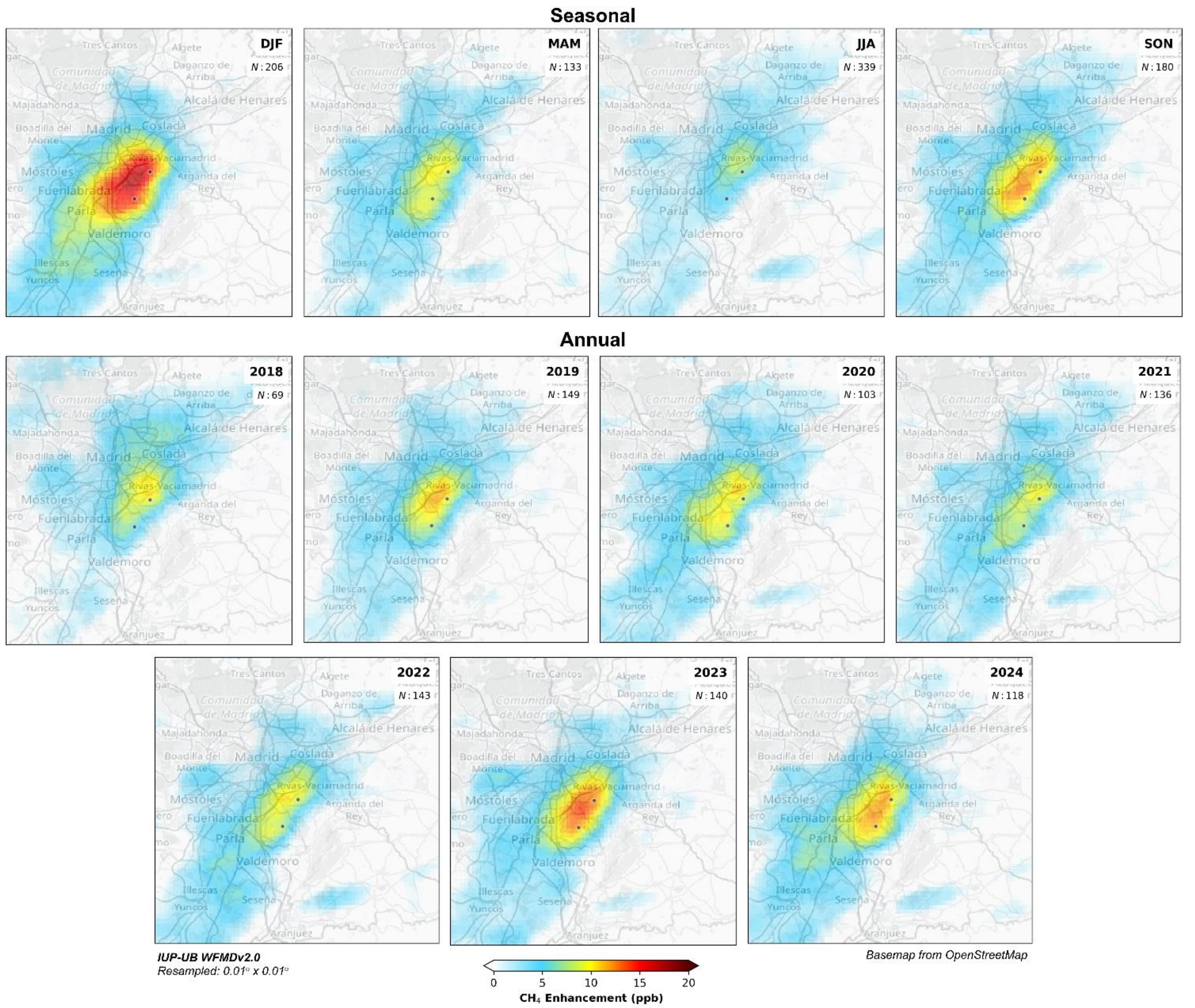

Figure A. 4: Seasonally (top row) and annually averaged CH_4 enhancement from the Sentinel-5P Bremen IUP-UB XCH_4 WFMD v2.0 product for years 2018-2024, where days with < 30% coverage of the domain were omitted.

https://doi.org/10.5194/egusphere-2026-3797
Preprint. Discussion started: 31 August 2026

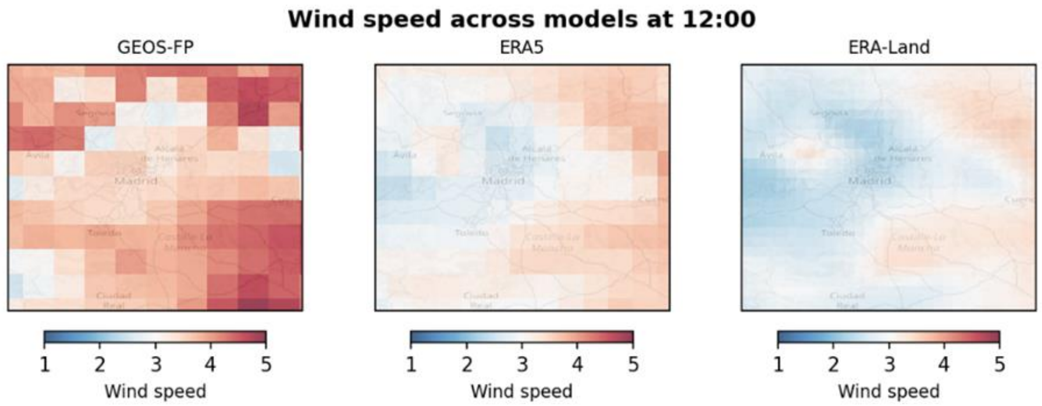

Figure A. 5: Averaged model wind speeds for Madrid at 12:00 UTC between 2020-2024 from GEOS-FP (left), ERA5 (centre) and ERA-Land (right) averaged on each models native grid all at a height of 10 m. Basemap: © OpenStreetMap

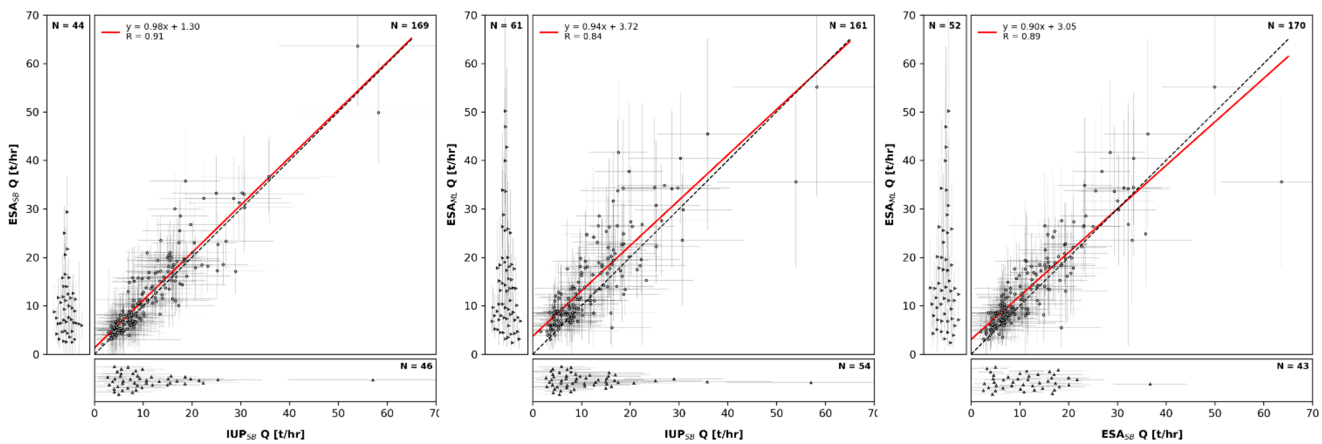

Figure A. 6: Correlation plots between TROPOMI emission products ESA_{SB}, ESA_{ML} and IUP_{SB}. Main panels show days where a plume is present in both datasets. Sub-panels show days where a plume was only detected in one of the two datasets.

https://doi.org/10.5194/egusphere-2026-3797
Preprint. Discussion started: 31 August 2026

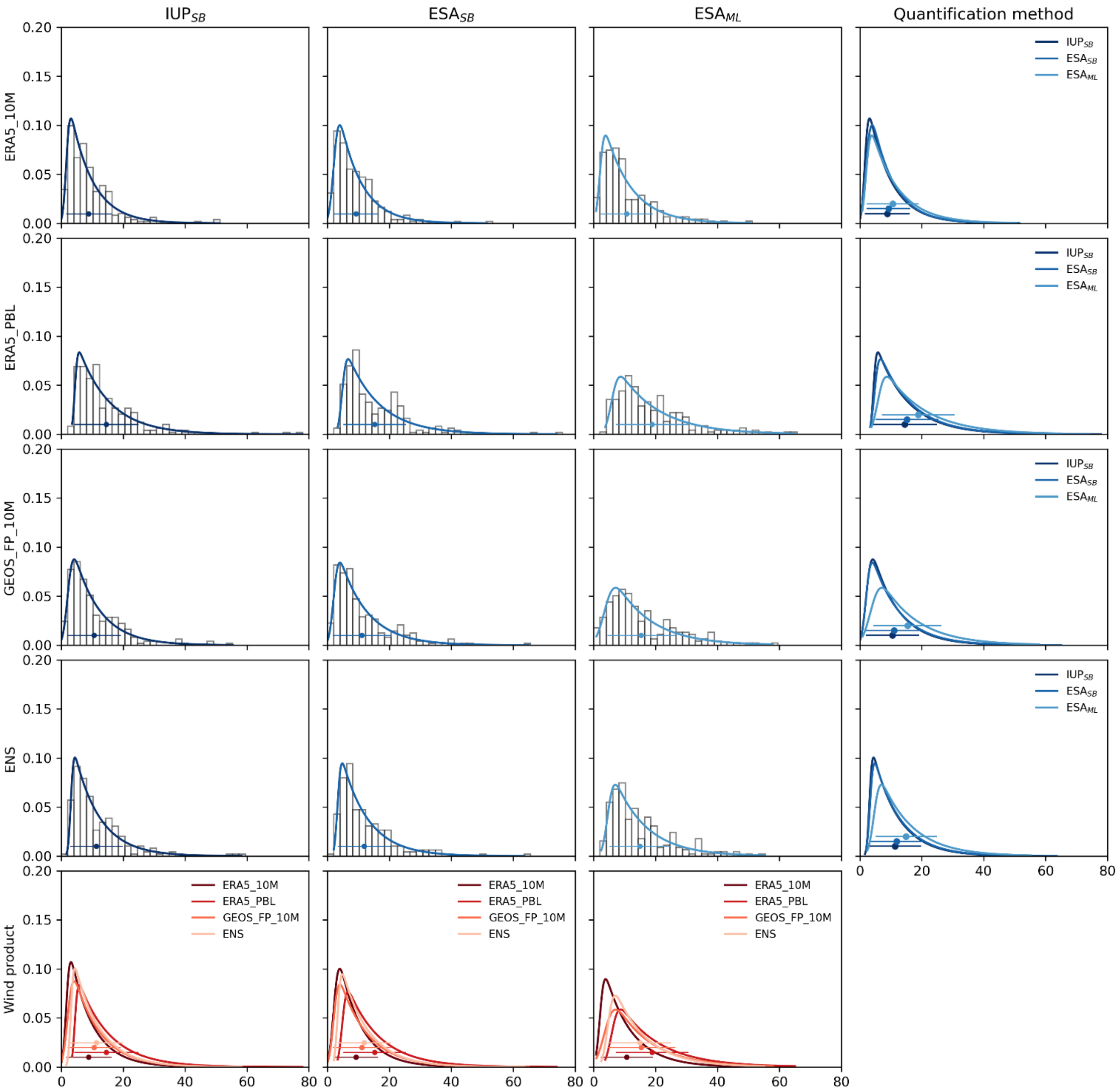

Figure A. 7: Emission (t/hr) distributions for each TROPOMI derived emission approach (shades of blue) and meteorlogical model (shades of red), with average and standard deviations shown below each distribution.

https://doi.org/10.5194/egusphere-2026-3797
Preprint. Discussion started: 31 August 2026

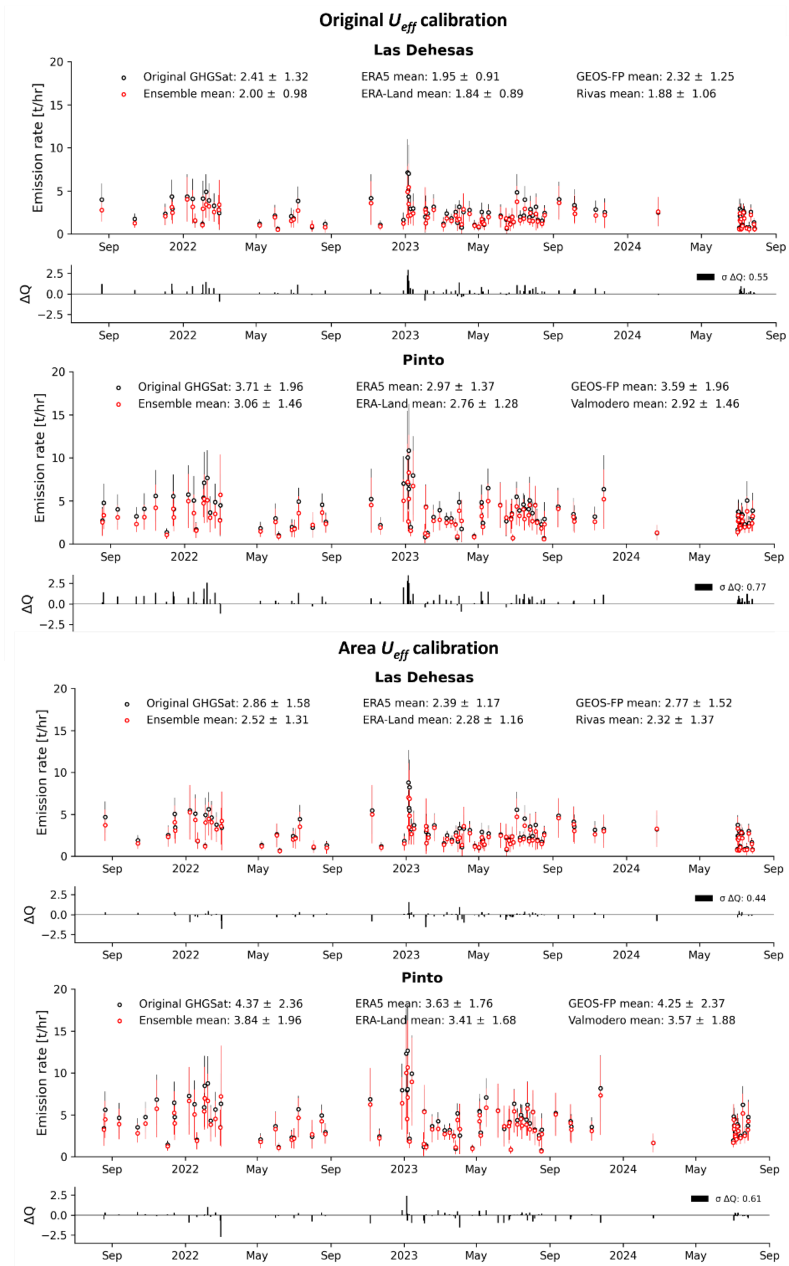

Figure A. 8: Recalculated GHGSat emission rates using emission rates delivered by GHGSat, as well as calculated from ERA5, ERA-Land, GEOS-FP, and nearby monitoring stations, using both the point source and area source calibration from Maasakkers et al (2022). ΔQ represents Original – Ensemble per plume.

https://doi.org/10.5194/egusphere-2026-3797
Preprint. Discussion started: 31 August 2026

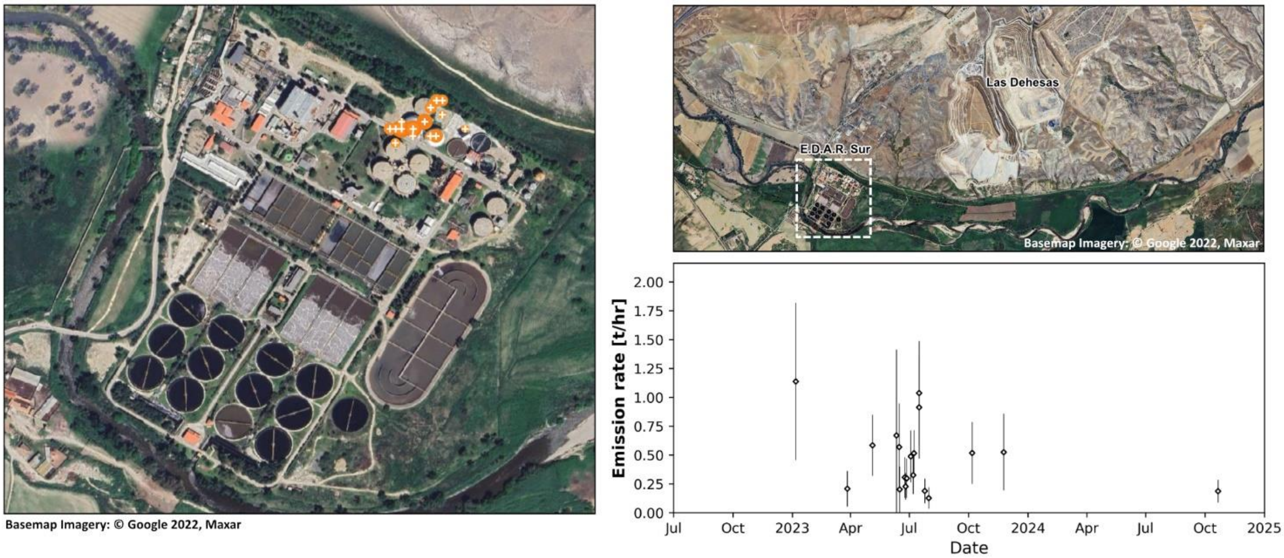

Figure A. 9: GHGSat observed emission plume origins and rates from E.D.A.R. Sur WWTP, with GHGSat plume origins (left), location relative to Las Dehesas (upper right), and emission time series (lower right).

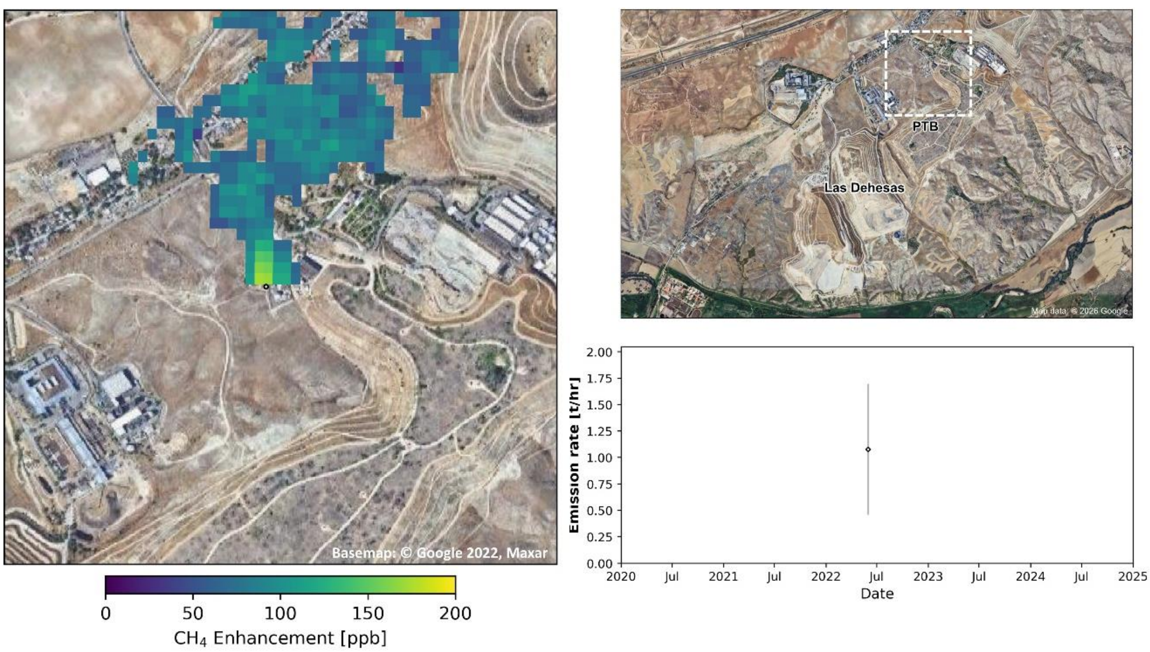

Figure A. 10: GHGSat observed emission plume from the PTB biogas upgrading facility (left), location relative to Las Dehesas (upper right), and emission rate (lower right).

https://doi.org/10.5194/egusphere-2026-3797
Preprint. Discussion started: 31 August 2026

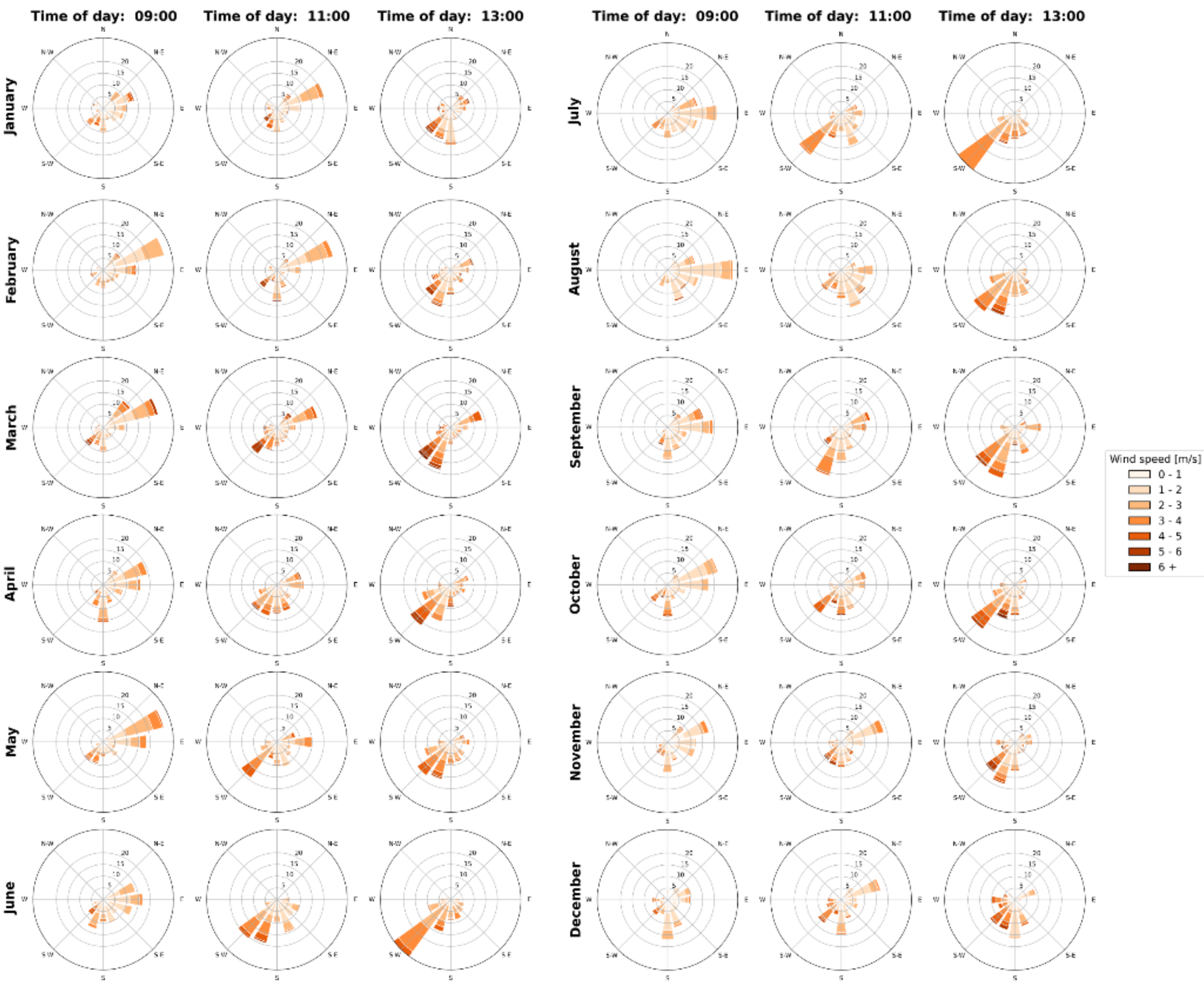

Figure A. 11: Wind rose of 2020-2024 winds from the Rivas-Vaciamadrid monitoring station averaged by month.